J. Fluid Mech. (1986), *vol.* 167, *pp.* 353–391
Printed in Great Britain

Chaotic streamlines in the ABC flows

By T. DOMBRE,
CNRS, Groupe de Physique des Solides, École Normale Supérieure
24 rue Lhomond, 75231 Paris Cedex 05, France

U. FRISCH,
CNRS, Observatoire de Nice, BP 139, 06003 Nice Cedex, France

J. M. GREENE,
GA Technologies Inc. PO Box 81608, San Diego,
California 92138, USA

M. HÉNON,
CNRS, Observatoire de Nice, BP 139, 06003 Nice Cedex, France

A. MEHR
Observatoire de Nice, BP 139, 06003 Nice Cedex, France

AND A. M. SOWARD
School of Mathematics, University of Newcastle upon Tyne,
Newcastle NE1 7RU, UK

(Received 15 May 1985 and in revised form 20 November 1985)

The particle paths of the Arnold–Beltrami–Childress (ABC) flows

$$\boldsymbol{u} = (A \sin z + C \cos y,\ B \sin x + A \cos z,\ C \sin y + B \cos x).$$

are investigated both analytically and numerically. This three-parameter family of spatially periodic flows provides a simple steady-state solution of Euler's equations. Nevertheless, the streamlines have a complicated Lagrangian structure which is studied here with dynamical systems tools. In general, there is a set of closed (on the torus, T^3) helical streamlines, each of which is surrounded by a finite region of KAM invariant surfaces. For certain values of the parameters strong resonances occur which disrupt the surfaces. The remaining space is occupied by chaotic particle paths: here stagnation points may occur and, when they do, they are connected by a web of heteroclinic streamlines.

When one of the parameters A, B or C vanishes the flow is integrable. In the neighbourhood, perturbation techniques can be used to predict strong resonances. A systematic search for integrable cases is done using Painlevé tests, i.e. studying complex-time singularities of fluid-particle trajectories. When $ABC \neq 0$ recursive clustering of complex time singularities occurs that seems characteristic of non-integrable behaviour.

1. Introduction

Three-dimensional steady flows with a simple Eulerian representation can have a chaotic Lagrangian structure. By this we mean that infinitesimally close fluid

particles following the streamlines may separate exponentially in time, while remaining in a bounded domain, and that individual streamlines may appear to fill entire regions of space (see also §3.1). Thus the positions of fluid particles may become effectively unpredictable for long times. A class of flows with presumably chaotic streamlines has been identified by Arnold (1965). These flows involve three real parameters A, B and C; relative to rectangular cartesian coordinates they are 2π-periodic in x, y, and z and have velocity $\boldsymbol{u} = (u, v, w)$, where

$$\left.\begin{aligned} u &= A\sin z + C\cos y, \\ v &= B\sin x + A\cos z, \\ w &= C\sin y + B\cos x. \end{aligned}\right\} \tag{1.1}$$

Arnold (1965) was interested in three-dimensional steady-state solutions of the Euler equation

$$\partial_t \boldsymbol{u} + \boldsymbol{\omega}\times\boldsymbol{u} = -\boldsymbol{\nabla} p_*, \tag{1.2}$$

where

$$p_* = p + \tfrac{1}{2}\boldsymbol{u}^2, \quad \boldsymbol{\omega} = \boldsymbol{\nabla}\times\boldsymbol{u}, \quad \boldsymbol{\nabla}\cdot\boldsymbol{u} = 0. \tag{1.3}$$

Streamlines lie on surfaces of constant p_* and therefore can only be chaotic in regions where p_* is constant, i.e. where the flow has the Beltrami properties:

$$\boldsymbol{\omega} = \lambda\boldsymbol{u}, \quad \boldsymbol{u}\cdot\boldsymbol{\nabla}\lambda = 0. \tag{1.4a,b}$$

Since (1.4b) implies that λ is constant in chaotic regions, periodic solutions are sought with, for simplicity, λ constant everywhere. Then the flow is a superposition of plane helical waves all having the same wavenumber $|\lambda|$ and all the same (right or left) circular polarization. With 2π-periodicity in x, y, and z assumed, it follows that $\lambda^2 = k^2+p^2+q^2$, where k, p, and q are unsigned integers. Any integer $n = \lambda^2$ which is not of the form $4^a(8b+7)$ – with a and b natural integers – may be written as the sum of three integer squares (see for example Landau 1927, theorem 187). It is thus possible to set up a great variety of Beltrami flows, most of which presumably have chaotic streamlines. It is not our purpose to explore all these flows. We just point out that they may be of interest in so far as they provide a large class of possible topologies for steady, spatially periodic solutions of the Euler (or magnetostatic) equation without recourse to 'non-analytic' solutions as in the work of Moffatt (1985) or Parker (1985). Henceforth we shall consider exclusively the simplest flows corresponding to Arnold's choice of (1.1); these have $\lambda^2 = 1$ and thus

$$(k, p, q) = (1, 0, 0) \quad \text{and permutations.} \tag{1.5}$$

Early numerical experiments by Hénon (1966) have provided evidence for chaos in the special case $A = \sqrt{3}$, $B = \sqrt{2}$, $C = 1$. The special case $A = B = C = 1$ was introduced independently by Childress (1967, 1970) as a model for the kinematic dynamo effect. We propose to call these flows ABC (for Arnold, Beltrami, Childress). Another study of a flow with a chaotic Lagrangian structure has been made by Arter (1983). He uses the Boussinesq model, with a buoyancy term in the momentum equation which is not a gradient; therefore the Beltrami property is not required for chaos.

From a *fluid dynamical* viewpoint flows with chaotic streamlines are interesting because they may considerably enhance transport without being turbulent in the usual sense – they only display what might be called 'Lagrangian turbulence'. Aref (1984) has shown that simple time-periodic two-dimensional flows can produce turbulent mixing of a passive scalar, limited only by the possible existence of Kolmogorov–Arnold–Moser (KAM) invariant surfaces. In three dimensions the same

is possible with steady flows such as the ABC's. Arnold *et al.* (1981) (see also Zel'dovich, Ruzmaikin & Sokolov 1983) noted that streamline chaos in a steady three-dimensional infinitely conducting flow favours the growth of magnetic fields (it is controlled by the largest Lyapunov exponent). Arnold & Korkina (1983), Galloway & Frisch (1984, 1986), and Moffatt & Proctor (1985) performed numerical and analytical studies of dynamo action at finite conductivity for the ABC flows.

In this paper we report our present knowledge of the kinematics of ABC flows. They have a very rich structure and may constitute a prototype for flows with chaotic streamlines.

The paper is organized as follows. In §2 we give some elementary facts about the ABC flows, a heuristic description of their morphology, and a qualitative explanation of why they are generally chaotic. In §3 the technique of Poincaré sections is used for detailed studies of the dynamical system defined by the trajectories of fluid particles; the flows exhibit a mixture of ordered regions (with KAM invariant surfaces) and chaotic regions (containing the unstable stagnation points), typical of conservative dynamical systems. Particular attention is paid to resonances disrupting the invariant surfaces. In §4 we study near-integrable cases, when one of the parameters A, B, C is small, using perturbation expansions. In §5 we make a systematic search for integrable cases using Painlevé tests. This involves going to complex times and studying singularities of fluid-particle trajectories. Such singularities are also important in so far as they determine the high-frequency and high-wavenumber behaviour of passive scalars (Frisch & Morf 1981). In §6 we study the complex time singularities in the non-integrable cases.

We note that in the present study, dynamical-systems concepts are relatively easy to translate into fluid-dynamical concepts since the flow is in physical space and not in some abstract phase space. Elementary introductions to conservative dynamical systems may be found in Helleman (1980) or Hénon (1983). More advanced material may be found in Arnold (1974, 1978), Moser (1973), Iooss, Helleman & Stora (1983) and Guckenheimer & Holmes (1983).

2. Overall structure

We are interested here in the structure of the three-dimensional flows given by (1.1). The Eulerian structure is straightforward. It consists of a superposition of three helical (left-polarized) Fourier modes depending respectively on x, y, and z. The ABC flows are divergenceless and satisfy the identity

$$\nabla \times \boldsymbol{u} = \boldsymbol{u}, \tag{2.1}$$

so that they have the Beltrami property and are exact solutions of the Euler equation (1.2).

Furthermore, the ABC flows may be considered as steady solutions of the Navier–Stokes equation

$$\partial_t \boldsymbol{u} + \boldsymbol{u}\cdot\nabla\boldsymbol{u} = -\nabla p + \nu\nabla^2\boldsymbol{u} + \boldsymbol{f}, \tag{2.2}$$

$$\nabla\cdot\boldsymbol{u} = 0, \quad \boldsymbol{u} \text{ to be } 2\pi\text{-periodic in } x, y, z, \tag{2.3}$$

with a force

$$\boldsymbol{f} = \nu(A\sin z + C\cos y, B\sin x + A\cos z, C\sin y + B\cos x). \tag{2.4}$$

When the viscosity ν is large, the ABC flow is the only stable solution of the Navier–Stokes equation (Galloway & Frisch 1985). As the viscosity is decreased,

bifurcations will take place, eventually leading to Eulerian turbulence. According to V. I. Arnold, (1985, private communication), this process may be enhanced here by the preexisting Lagrangian turbulence; this was his original motivation for introducing the ABC flows.

2.1. *The dynamical system*

The difficulties start with questions involving the Lagrangian structure. What is the global structure of streamlines or vortex lines? How is a passive scalar undergoing pure advection transported by the flow? For this we must study the dynamical system associated with fluid particle motion:

$$\dot{x} = A \sin z + C \cos y, \tag{2.5a}$$

$$\dot{y} = B \sin x + A \cos z, \tag{2.5b}$$

$$\dot{z} = C \sin y + B \cos x. \tag{2.5c}$$

For real A, B, C and real $\boldsymbol{x}(0)$ there is a unique solution $\boldsymbol{x}(t)$ for all real t. The map $\boldsymbol{x}(0) \mapsto \boldsymbol{x}(t)$ defines a conservative (i.e. volume preserving) dynamical system. The Eulerian flow is 2π-periodic in x, y, and z; thus the map commutes with 2π translations in x, y, and z. It is important to distinguish between the problem where $\boldsymbol{x}$ is in $\mathbf{R}^3$ and where $\boldsymbol{x}$ is in the torus $\mathbf{T}^3$ (in the latter case coordinates are defined modulo 2π). In this paper we shall adopt the $\mathbf{T}^3$ viewpoint unless otherwise stated, with our attention restricted to a *periodicity box* which we shall choose to be the cube

$$0 \leqslant x \leqslant 2\pi, \quad 0 \leqslant y \leqslant 2\pi, \quad 0 \leqslant z \leqslant 2\pi. \tag{2.6}$$

2.2. *Symmetries*

The equations (2.5) have a number of internal symmetries. They are invariant under each of the following three transformations:

$$\left.\begin{array}{lllll} S_1\colon & x' = x, & y' = \pi - y, & z' = -z, & t' = -t; \\ S_2\colon & x' = -x, & y' = y, & z' = \pi - z, & t' = -t; \\ S_3\colon & x' = \pi - x, & y' = -y, & z' = z, & t' = -t. \end{array}\right\} \tag{2.7}$$

Each of these transformations is a symmetry with respect to an axis. These symmetries relate time-reversed streamlines; flows that have such symmetries are called reversible (Birkhoff 1927).

On combining with the periodicity properties, one finds that the system has actually an infinite number of axes of symmetry. In the case of S_1, for instance, these axes are parallel to the x-direction and located at

$$y = \tfrac{1}{2}\pi + \pi j_2, \quad z = \pi j_3, \tag{2.8}$$

where j_2 and j_3 are arbitrary integers. Similar equations are obtained for S_2 and S_3 by cyclic permutation of the coordinates.

Six axes of symmetry are shown on figure 1. They lie on the faces of the cube

$$0 \leqslant x \leqslant \pi, \quad 0 \leqslant y \leqslant \pi, \quad 0 \leqslant z \leqslant \pi, \tag{2.9}$$

which will be called the *fundamental box*. All other axes are obtained by replicating this cube periodically in x, y and z.

The three symmetries S_1, S_2, S_3 commute (modulo 2π) and the square of each is the identity; therefore they generate a group of eight elements, the direct product

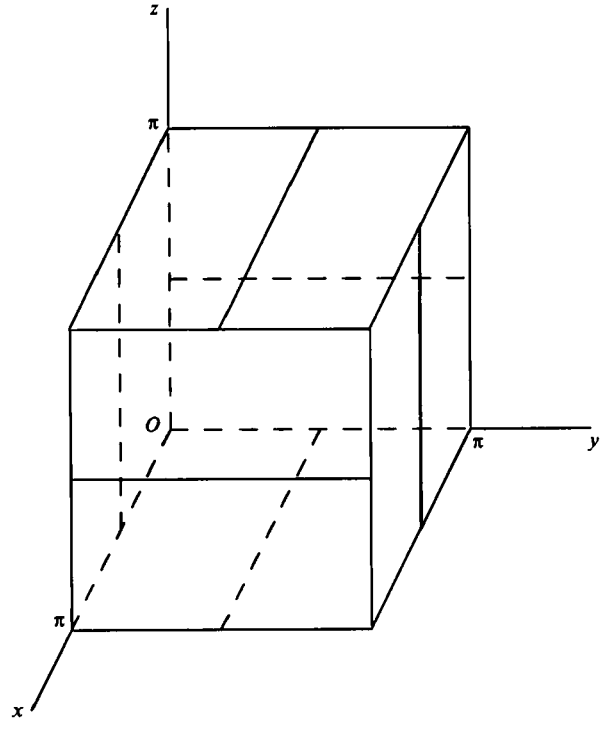

FIGURE 1. Fundamental box and axes of symmetry.

$C_2 \times C_2 \times C_2$ where C_2 is the cyclic group of two elements. The five remaining elements are:

$$\left.\begin{array}{rl} I: & \textit{identity}; \\ S_2S_1: & x' = -x, \quad y' = \pi - y, \quad z' = \pi + z, \quad t' = t; \\ S_3S_2: & x' = \pi + x, \quad y' = -y, \quad z' = \pi - z, \quad t' = t; \\ S_1S_3: & x' = \pi - x, \quad y' = \pi + y, \quad z' = -z, \quad t' = t; \\ S_3S_2S_1: & x' = \pi + x, \quad y' = \pi + y, \quad z' = \pi + z, \quad t' = -t. \end{array}\right\} \tag{2.10}$$

Note that the transformations S_2S_1, S_3S_2 and S_1S_3 commute with the fluid-particle motion defined by (2.5). Only two of them are independent, since each is the product of the other two.

The periodicity box can be divided into eight smaller cubes, each of which is the image of the fundamental box under one of the above eight symmetries. Therefore we could, in principle, restrict our attention to the fundamental box. In practice this is not very convenient, however, because the effect of the combined symmetries is not easy to visualize. So we shall generally work with the periodicity box.

If we consider the whole class of ABC flows and allow the parameters A, B, C to change, a number of additional symmetries emerge. They will allow a reduction of the region to be considered in parameter space.

(i) The equations are invariant under the transformation

$$A' = -A, \quad z' = z + \pi. \tag{2.11}$$

We can therefore assume $A \geqslant 0$. Similar transformations allow a reduction to $B \geqslant 0$ and $C \geqslant 0$.

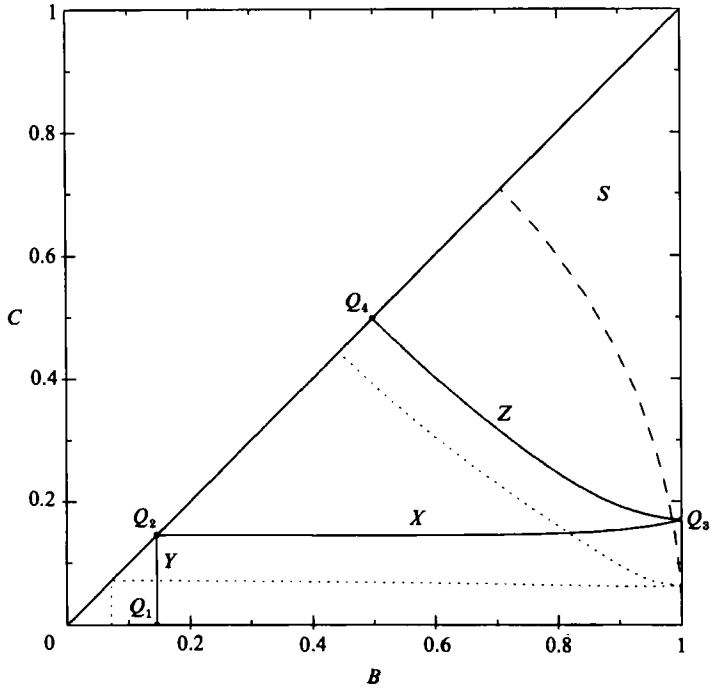

FIGURE 2. Restricted parameter space, defined by (2.15): ---, boundary of S, the region of existence of stagnation points; ——, locus of 3:1 resonances; · · · ·, locus of 4:1 resonances.

(ii) The equations are invariant under the cyclic permutation

$$A' = B, \quad B' = C, \quad C' = A, \quad x' = y, \quad y' = z, \quad z' = x. \tag{2.12}$$

We can therefore assume that A is the largest of the three parameters: $A \geqslant B$ and $A \geqslant C$.

(iii) The equations are invariant under

$$B' = C, \quad C' = B, \quad x' = \tfrac{3}{2}\pi - y, \quad y' = \tfrac{3}{2}\pi - x, \quad z' = \tfrac{3}{2}\pi - z. \tag{2.13}$$

We can therefore assume that $B \geqslant C$.

(iv) The equations are invariant under

$$A' = \mu A, \quad B' = \mu B, \quad C' = \mu C, \quad t' = t/\mu, \tag{2.14}$$

where μ is an arbitrary constant. We can therefore normalize to $A = 1$ (unless all three parameters vanish).

These four steps result in the following restriction of the parameters:

$$1 = A \geqslant B \geqslant C \geqslant 0. \tag{2.15}$$

The restricted parameter space is thus a triangle in the (B, C)-plane (figure 2).

Finally we note that the symmetries for the case $A = B = C = 1$ have been investigated by Arnold (1984). In particular he showed that the symmetry group (not including time-reversing transformations) contains 24 elements and is isomorphic to the rotation group of the cube. His results are consistent with ours.

2.3. *Stagnation points*

One of the features of the ABC flows is that they may have stagnation points where the fluid velocity (and vorticity) vanish. It is straightforward to solve for the location of these points, with the result

$$\left.\begin{aligned} -C\sin y = B\cos x &= \pm[\tfrac{1}{2}(B^2+C^2-A^2)]^{\frac{1}{2}},\\ -A\sin z = C\cos y &= \pm[\tfrac{1}{2}(C^2+A^2-B^2)]^{\frac{1}{2}},\\ -B\sin x = A\cos z &= \pm[\tfrac{1}{2}(A^2+B^2-C^2)]^{\frac{1}{2}}. \end{aligned}\right\} \tag{2.16}$$

the condition that x, y, and z all be real is that a triangle can be formed with sides A^2, B^2 and C^2. Then there are eight stagnation points in the periodicity box or, equivalently, one in the fundamental box. Within the parameter space defined by (2.15), the triangle inequality reduces to

$$B^2+C^2 \geqslant 1, \tag{2.17}$$

which defines the region S (for stagnation points) illustrated in figure 2. Notice that it has a cusp touching the integrable case $C = 0$ (see §2.4) at $B = 1$.

Let us examine the local behaviour around a stagnation point $\boldsymbol{x}_s$. Setting $\tilde{\boldsymbol{x}} = \boldsymbol{x}-\boldsymbol{x}_s$, we have, for small $\tilde{\boldsymbol{x}}$,

$$\frac{\mathrm{d}\tilde{\boldsymbol{x}}}{\mathrm{d}t} = \boldsymbol{\nabla u}_s\,\tilde{\boldsymbol{x}}, \tag{2.18}$$

where $\boldsymbol{\nabla u}_s$ is the velocity gradient matrix evaluated at the stagnation point. It is symmetrical since its antisymmetrical part is related to the vorticity which also vanishes at the stagnation point. Hence the eigenvalues of $\boldsymbol{\nabla u}_s$, solutions of the characteristic equation

$$\lambda^3-\tfrac{1}{2}(A^2+B^2+C^2)\,\lambda-2ABC\cos x\cos y\cos z = 0, \tag{2.19}$$

are real. It is easily checked that they are always distinct except in the particular case $A = B = C$. The absence of a λ^2 term in (2.19) reflects the fact that

$$\boldsymbol{\nabla}\cdot\boldsymbol{u}_s = \mathrm{Tr}\,(\boldsymbol{\nabla u}_s) = 0 \tag{2.20}$$

and implies that the eigenvalues sum to zero. Consequently two eigenvalues of $\boldsymbol{\nabla u}_s$ have one sign and the third has the other sign. Therefore the stagnation points are unstable fixed points of the dynamical system (2.5). Following Cowley (1973), who considered a similar problem in studying the three-dimensional structure of magnetic field lines, we classify stagnation points with two negative eigenvalues as type α (rather than A in Cowley, to avoid confusion) and those with two positive eigenvalues as type β. We notice that when parameters are changed, stagnation points are created or destroyed in $\alpha\beta$ pairs as (B, C) crosses the circle $B^2+C^2 = 1$.

When the eight stagnation points exist, the one in the fundamental box is always of type β. The seven other stagnation points can be deduced using the group of symmetries discussed in §2.2. In so doing, a change of sign in t signifies a change of sign of the eigenvalues, i.e. a change from type α to type β or the converse.

2.4. *An integrable case*

The equations governing fluid-particle motion are in general not integrable. There is however at least one obvious exception, namely the case $C = 0$, for which

$$\dot{x} = A\sin z, \quad \dot{y} = B\sin x + A\cos z, \quad \dot{z} = B\cos x. \tag{2.21a,b,c}$$

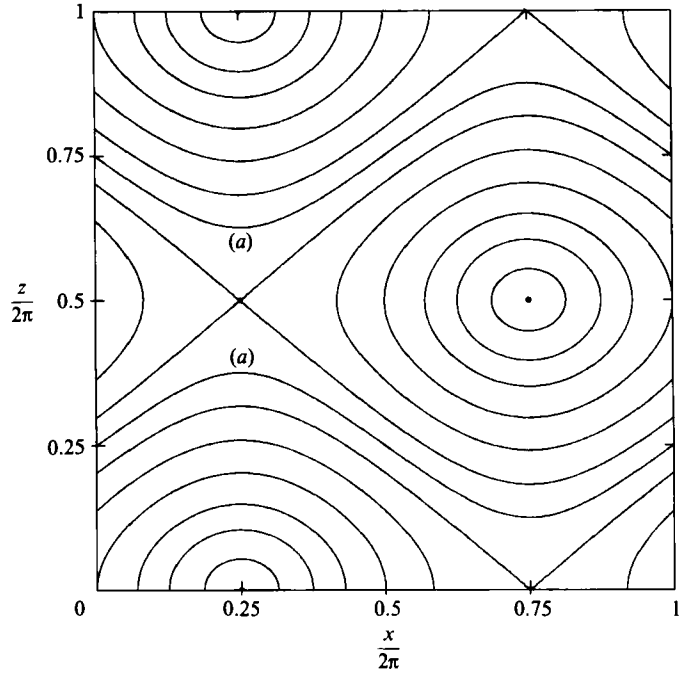

FIGURE 3. The integrable case: projection of streamlines on (x, z)-plane.

The first and third equations form a separable system. By elimination of the time, this system is immediately integrated into

$$B \sin x + A \cos z = V, \tag{2.22}$$

where V is a constant. By further integration (see Appendix A) $x(t)$ and $z(t)$ can be expressed as elliptic integrals. Finally, since the integral (2.22) is identical with the right-hand side of (2.21*b*), the y-motion is simply

$$y = y_0 + Vt. \tag{2.23}$$

Our results show that the particular case $C = 0$ is separable and integrable. The streamlines in the (x, z)-plane are represented on figure 3. The motion consists of a circulation along one of the curves of figure 3, accompanied by a uniform motion in y. The figure shows circulation in four 'cells' each of which in $\mathbf{T}^3$ is topologically a set of nested tori. In two of these, with an elliptical structure, the flow is along and around a central axis, the closed streamline at the centre. Such cells will be called 'vortices'. The other two cells (wavy lines joining $x = 0$ to $x = 2\pi$) are 'shear layers'. In the centre of the lower shear layer is a surface formed of streamlines that close after circulating once in the x-direction. Above and below this surface the flow has an additional component in the negative or positive y-direction. A winding number can be defined in the shear layer as the number of loops in the y-direction divided by the number of loops in the x-direction. This winding number varies continuously from $-\infty$ to $+\infty$, and streamlines are closed wherever it is rational.

2.5. *The six principal vortices*

Numerical computations (§3) suggest that there exist regions of space where the flow is predominantly in one direction. Each of these regions has roughly the shape of a

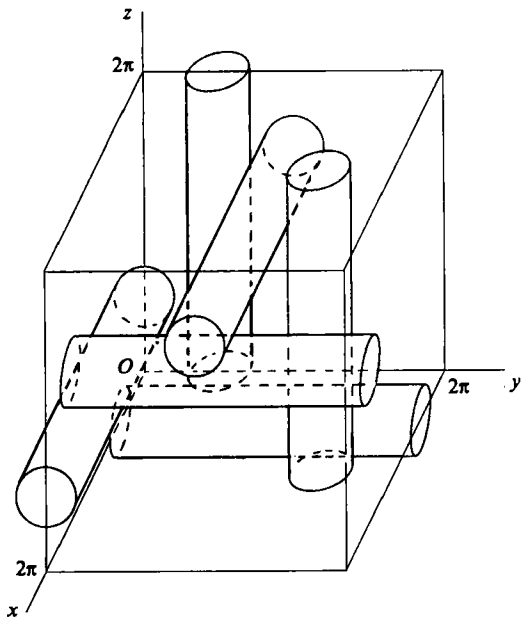

FIGURE 4. Sketch of the six principal vortices.

tube parallel to one of the three axes, and will be called a *principal vortex*, or a *vortex* for short. We show here how the existence of these vortices can be derived from a naive analysis of (2.5*a–c*). A more systematic perturbation analysis, valid near the integrable case, will be presented in §4.

We look for a region where the motion is predominantly in one direction, for example the y-direction; this will be called a y-vortex. We try therefore to maximize $\dot{y}$. This gives

$$x \simeq \tfrac{1}{2}\pi, \quad z \simeq 0. \tag{2.24}$$

Integrating (2.5*b*), we obtain

$$y \simeq (A+B)\,t. \tag{2.25}$$

Equations (2.5*a*,*c*) then reduce to

$$\dot{x} \simeq C\cos y, \quad \dot{z} \simeq C\sin y. \tag{2.26}$$

Since $\dot{x}$ and $\dot{z}$ are zero on the average, it is conceivable that the conditions (2.24) will remain satisfied along a streamline. In a similar way, by considering the five other possible directions (we can specify both the axis x, y, or z and the sign), we obtain a total of six vortices; their arrangement is sketched on figure 4.

We can go a little further and derive to first order the excursions of x and z from their mean values (2.24). Instead of (2.26) we write

$$\left.\begin{aligned} \dot{x} &\simeq C\cos[(A+B)\,t]+Az, \\ \dot{z} &\simeq C\sin[(A+B)\,t]-B(x-\tfrac{1}{2}\pi). \end{aligned}\right\} \tag{2.27}$$

This has the general solution

$$\left.\begin{aligned} x-\tfrac{1}{2}\pi &\simeq \frac{BC}{A^2+AB+B^2}\sin[(A+B)\,t]+\alpha A^{\frac{1}{2}}\sin[(AB)^{\frac{1}{2}}t-\phi], \\ z &\simeq -\frac{AC}{A^2+AB+B^2}\cos[(A+B)\,t]+\alpha B^{\frac{1}{2}}\cos[(AB)^{\frac{1}{2}}t-\phi], \end{aligned}\right\} \tag{2.28}$$

where α and ϕ are constants of integration. The first terms in the right-hand sides represent the driven oscillation, i.e. the shape of the vortex as a whole. Thus, the vortex is not straight, but twisted into the shape of a left-handed helix making one turn when y increases by 2π. (No attempt was made to represent this on figure 4.)

It can be seen that the shape and phase of this helical motion are such that vortices adapt to the existence of other vortices so as to avoid each other. Because of this effect, the vortices can have a larger cross-section without intersecting each other.

The second terms in (2.28) represent the departure of a particular streamline from the vortex axis; this is itself helical, but the helicity is opposite to that of the vortex axis. We shall come back to this in §4.1 using more systematic perturbation theory.

2.6. *Separatrices and chaos*

Our aim is to understand at least heuristically why the ABC flows display chaotic features outside of the principal vortices. We believe that much can be understood in terms of unstable periodic orbits and fixed points. The former are closed hyperbolic streamlines; the latter are stagnation points.

Let us begin with near-integrable cases without stagnation points which lie just above the line $C = 0$ but outside the cusp-shaped region of figure 2. In this case the appearance of chaos is qualitatively understood in terms of homoclinic orbits. This goes back to Poincaré's (1982) work. We notice that in the integrable case there are closed unstable streamlines going through X points. For example in figure 3, the point $x = \frac{1}{2}\pi$, $z = \pi$ is the junction of four different flow cells. The corresponding streamline will be called a junction streamline. Figure 3 also shows that the flow cells are bounded by the sheets of streamlines that diverge from the junction streamline and converge back after going around. Such lines are therefore homoclinic (by definition). In the integrable case, homoclinic lines form two-dimensional sheets in the three-dimensional flow. In the perturbed case, the unstable closed junction streamlines still exist, and there are sheets of streamlines that asymptotically converge or diverge from each of these junction streamlines, called respectively the stable manifold and the unstable manifold of the junction streamline. Near a junction streamline the stable manifold serves as a separatrix of fluid particles that diverge from the junction streamline in opposite directions. Away from the junction streamline the picture becomes complicated. Indeed what is different in the non-integrable case is that the stable and unstable manifolds of the junction streamline are no longer coincident but intersect repeatedly along homoclinic streamlines. This was shown by Gautero (1985) for the ABC flows using the method of Melnikov (1963). Each unstable manifold becomes infinitely folded up against itself after going around the torus (see e.g. figures 36–39 in Hénon 1983). In the bounded region of folding the infinite convolution of the stable and unstable manifolds provides an efficient mixing mechanism for fluid particles after many eddy-circulation times. We stress that a detailed quantitative understanding of this kind of chaos is still lacking.

The case with stagnation points inside the cusp-shaped region S on figure 2 is quite different. From the viewpoint of Hamiltonian systems with two degrees of freedom this situation is not structurally stable. It is, however, when we consider the flow generated by a three-dimensional vector field of zero divergence: under a small perturbation the zeros of the vector field will be just slightly displaced.

Here we give a first attempt at understanding the topological structure associated with stagnation points. A type-α (in the sense of §2.3) stagnation point has a two-dimensional stable manifold made of the sheet of streamlines that asymptotically approach the stagnation point. Similarly, a type-β stagnation point has a two-

dimensional unstable manifold. Locally stable manifolds act as separatrices. Now, consider a point M on the intersection of two sheets associated with type-α and type-β stagnation points respectively (assuming such an intersection exists). Since each sheet is composed of streamlines, the flow cannot have a component perpendicular to either sheet. Thus the streamline through M lies entirely on the intersection of the two sheets. Since each line in one sheet must diverge from a β-point, and each line in the other sheet must converge toward an α-point, this particular streamline joins β- to α-points. It is therefore a heteroclinic line, or *null–null line* (Greene 1982).

It takes a fluid particle an infinite time (from $-\infty$ to $+\infty$) to travel a heteroclinic line from a type-β to a type-α stagnation point. Each individual heteroclinic line appears to have a fairly simple structure (see §3.3). Notice however that the stable and unstable manifolds may wrap around the $\mathbf{T}^3$ torus in a very complicated way, so that their intersections may form a complicated web of heteroclinic lines. We conjecture, at least for the ABC flows, that there are infinitely many heteroclinic lines joining two stagnation points of different types; these increasingly wrap around the $\mathbf{T}^3$ torus. Some supporting numerical evidence will be given in §3.3. This structure may play a role in the generation of chaos when stagnation points are present. An interesting phenomenon happens when two stagnation points annihilate by coalescing in a saddle-node bifurcation: the shortest heteroclinic line disappears, while the other ones go over into unstable periodic orbits. This is shown in Appendix B. Similar phenomena have been discussed by Šil'nikov (1969) and C. Tresser (1984, private communication).

3. Numerical experiments

3.1. *Flow visualization by Poincaré sections*

The purpose of this Section is to provide detailed visualization of the Lagrangian structure of the ABC flows by numerical techniques. Three-dimensional visualization techniques (e.g. stereo perspectives) are appropriate for discrete collections of points, lines or surfaces, but not for the streamlines of three-dimensional vector fields. We shall resort to a standard technique in dynamical systems originally introduced as a mathematical tool by Poincaré (1892) for problems of celestial mechanics. The method of Poincaré sections is a two-dimensional coding of the three-dimensional dynamical system in which one represents only the successive intersections of streamlines with one or several surfaces of sections (usually planes). This has the advantage that it clearly brings out the relevant objects (KAM surfaces, chaotic regions, resonances, etc.) as we shall now see. The basic equations (2.5) are considered as a dynamical system on $\mathbf{T}^3$ with x, y, and z defined modulo 2π and the parameters A, B and C normalized as in (2.15).

Figure 5 shows a typical example of a Poincaré section, for the case $A^2 = 1$, $B^2 = \frac{2}{3}$, $C^2 = \frac{1}{3}$ already studied by Hénon (1966). Several streamlines are represented. For each streamline, many successive intersections with the surface of section $z = 0$ are represented. The usual features of non-integrable Hamiltonian systems with two degrees of freedom are apparent. The plane is essentially divided into 'ordered' and 'chaotic' regions. In ordered regions, successive points belonging to the same streamline lie on a well-defined curve. In three-dimensional space, therefore, the streamline itself lies on a two-dimensional surface, namely a KAM surface. In chaotic regions, on the other hand, the points seem to be randomly scattered over a two-dimensional region. All scattered points on figure 5 correspond in fact to a single

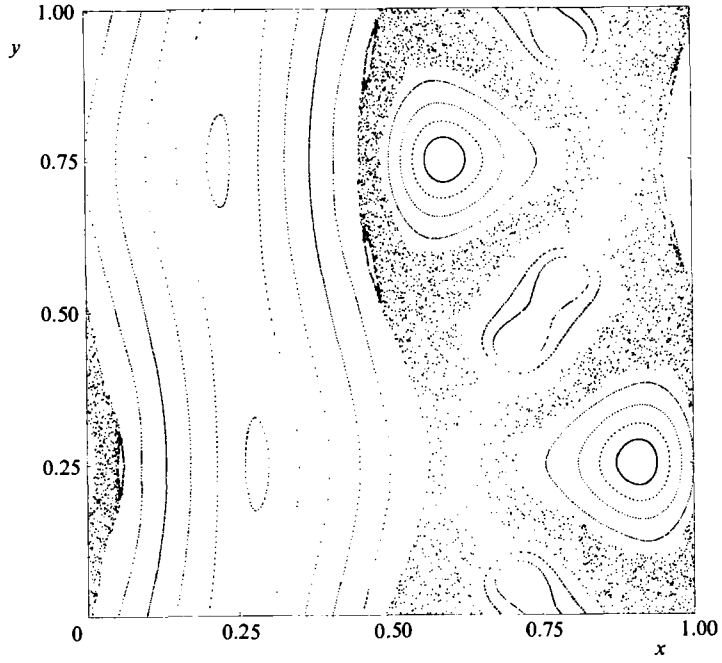

FIGURE 5. A typical Poincaré section, for the case $A^2 = 1$, $B^2 = \frac{2}{3}$, $C^2 = \frac{1}{3}$.

streamline, for which 5×10^3 successive interactions have been computed. This indicates that the streamline itself wanders in a three-dimensional region of space, which it fills more and more densely as time goes on.

In order to give a better idea of the three-dimensional structure of the flow, a number of Poincaré sections will now be shown simultaneously. The standard arrangement is represented in figure 6. There are eight equidistant sections parallel to the (y, z)-coordinate system, corresponding to $x = 0, \frac{1}{4}\pi, \ldots, \frac{7}{4}\pi$, and similarly for the other directions – a total of 24 sections.

Figure 7 represents in this way a single chaotic streamline, starting from $x = y = z = 0$, again for the case $A^2 = 1$, $B^2 = \frac{2}{3}$, $C^2 = \frac{1}{3}$. A total of approximately 10^5 points are represented.

The density of the points is not uniform; this is easily explained. Consider for instance a small region with area σ in one of the surfaces of section $y = \text{const.}$, and a small cylinder parallel to the local direction of flow, with base σ and height $\dot{y}\,\mathrm{d}t$. At the next intersection with the same surface of section, the image of this cylinder is another cylinder of base σ' and height $\dot{y}'\,\mathrm{d}t$. Volumes in (x, y, z) are preserved by the flow; therefore $\sigma\dot{y}\,\mathrm{d}t = \sigma'\dot{y}'\,\mathrm{d}t$. Thus σ varies as the inverse of $\dot{y}$. It follows that the density of the points in a surface of section is proportional to $\dot{y}$, the perpendicular component of velocity. In particular, the density falls to zero along the line defined by $\dot{y} = 0$, or

$$B \sin x + A \cos z = 0. \tag{3.1}$$

This line is the locus of the points where streamlines are tangential to the surface of section. The line (3.1), and the equivalent lines for the other directions of section, are represented on figure 8 for the same values of A, B, C as in figure 7.

The empty regions in figure 7 are the ordered regions. They can be seen to

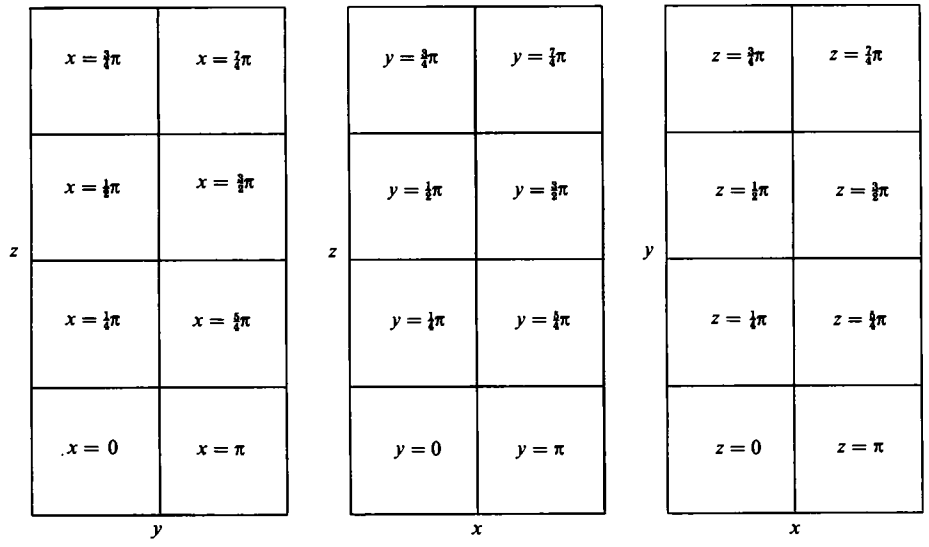

FIGURE 6. Key for figures 7–13.

correspond with the six principal vortices (§2.5). Figure 9 shows details for the case of the vortex for which x is constantly decreasing. A number of streamlines are represented. The x-sections (left) illustrate the structure of this vortex most clearly. The analysis of §2.5 is confirmed: at lowest order, the vortex is a cylinder, with its axis in $y = \pi$, $z = \frac{3}{2}\pi$; at next order, the vortex is a left-handed helix, the excursions in y and z being proportional to $\cos x$ and $-\sin x$ respectively.

A given streamline describes a helicoidal motion on the surface of the vortex, which should not be confused with the motion of the vortex itself. It is characterized by a *winding number*, which is the fraction of a turn made by the helix when x decreases by 2π. This winding number can take arbitrary values. This kind of streamline is called a *quasi-periodic orbit*.

A set of two islands can be seen among the nested curves. It corresponds to a streamline for which the winding number is exactly $\frac{1}{2}$: each island comes back to itself when x has decreased by 4π. An examination of the successive x-sections shows also that the streamline has the shape of a right-handed helix: it rotates in the direction opposite to that of the vortex itself (see §§2.5 and 4).

Sets of streamlines similar to figure 9 are found in the five other principal vortices.

A single chaotic streamline is represented in figure 10 for the particular case $A^2 = B^2 = C^2 = 1$ introduced by Childress (1967, 1970) for dynamo studies. When compared with figure 7 the chaotic region is small but appears more complex. New empty regions appear which are again occupied by quasi-periodic streamlines, as could be expected. These streamlines, however, are no longer associated with any of the six principal vortices. In the example illustrated by figure 11 the numbers indicate the order in which some sections are encountered; this gives an idea of the motion in (x, y, z)-space (number 12 is followed by number 1). For each coordinate, the motion can be described as the superposition of an oscillation and a steady progression; after one period, x and y have increased by 2π while z has decreased by 2π. Seven additional chaotic streamlines can be obtained by applying the symmetries described in §2. The eight streamlines, taken together, occupy all the smaller empty regions of figure 10. These streamlines belong to what we shall call *secondary vortices*.

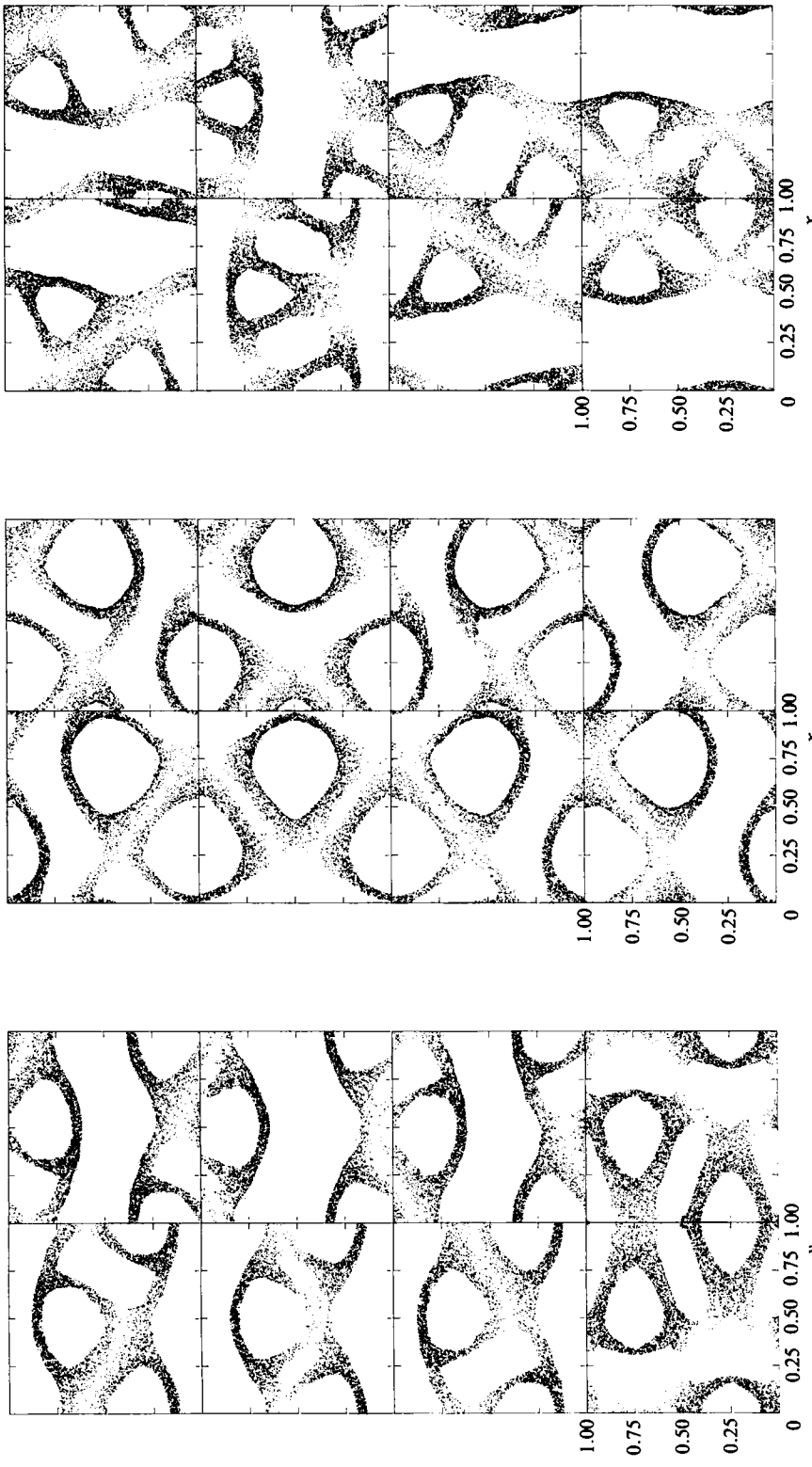

FIGURE 7. Poincaré section for a single streamline filling a chaotic region; $A^2 = 1$, $B^2 = \frac{2}{3}$, $C^2 = \frac{1}{3}$.

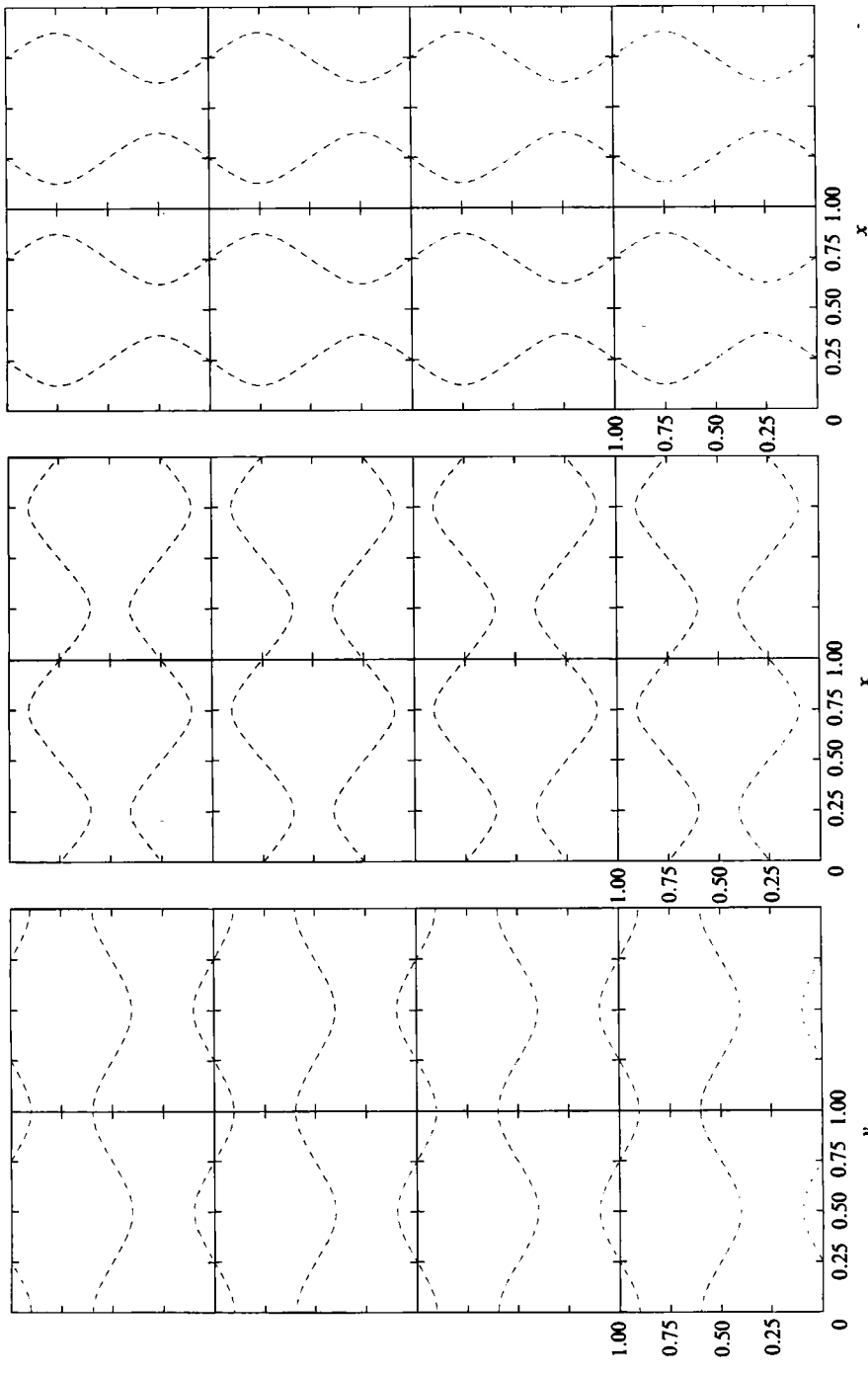

FIGURE 8. Loci of points where streamlines are tangential to the surface of section, for $A^2 = 1$, $B^2 = \frac{2}{3}$, $C^2 = \frac{1}{3}$.

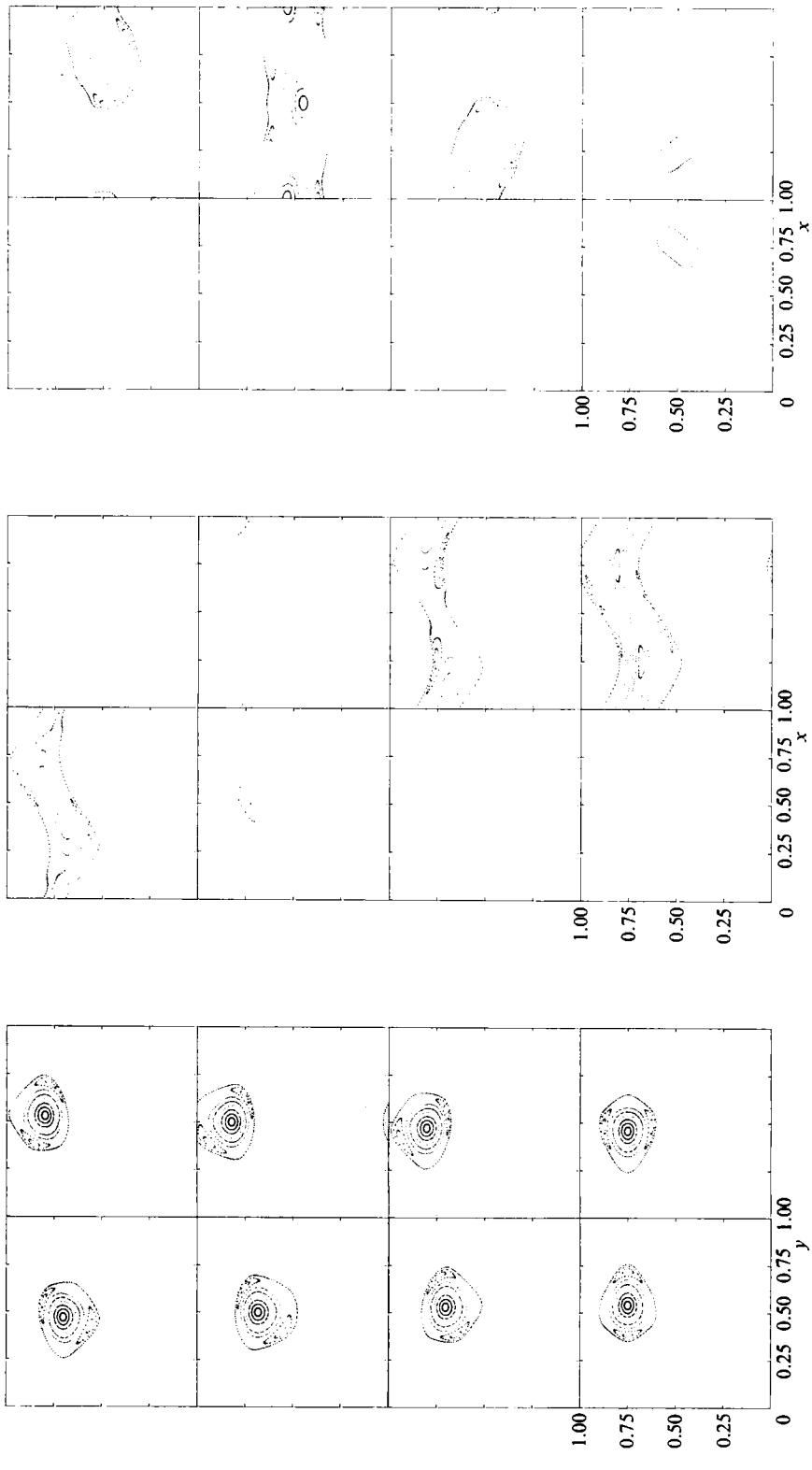

FIGURE 9. Poincaré section of a main vortex, for $A^2 = 1$, $B^2 = \frac{2}{3}$, $C^2 = \frac{1}{3}$.

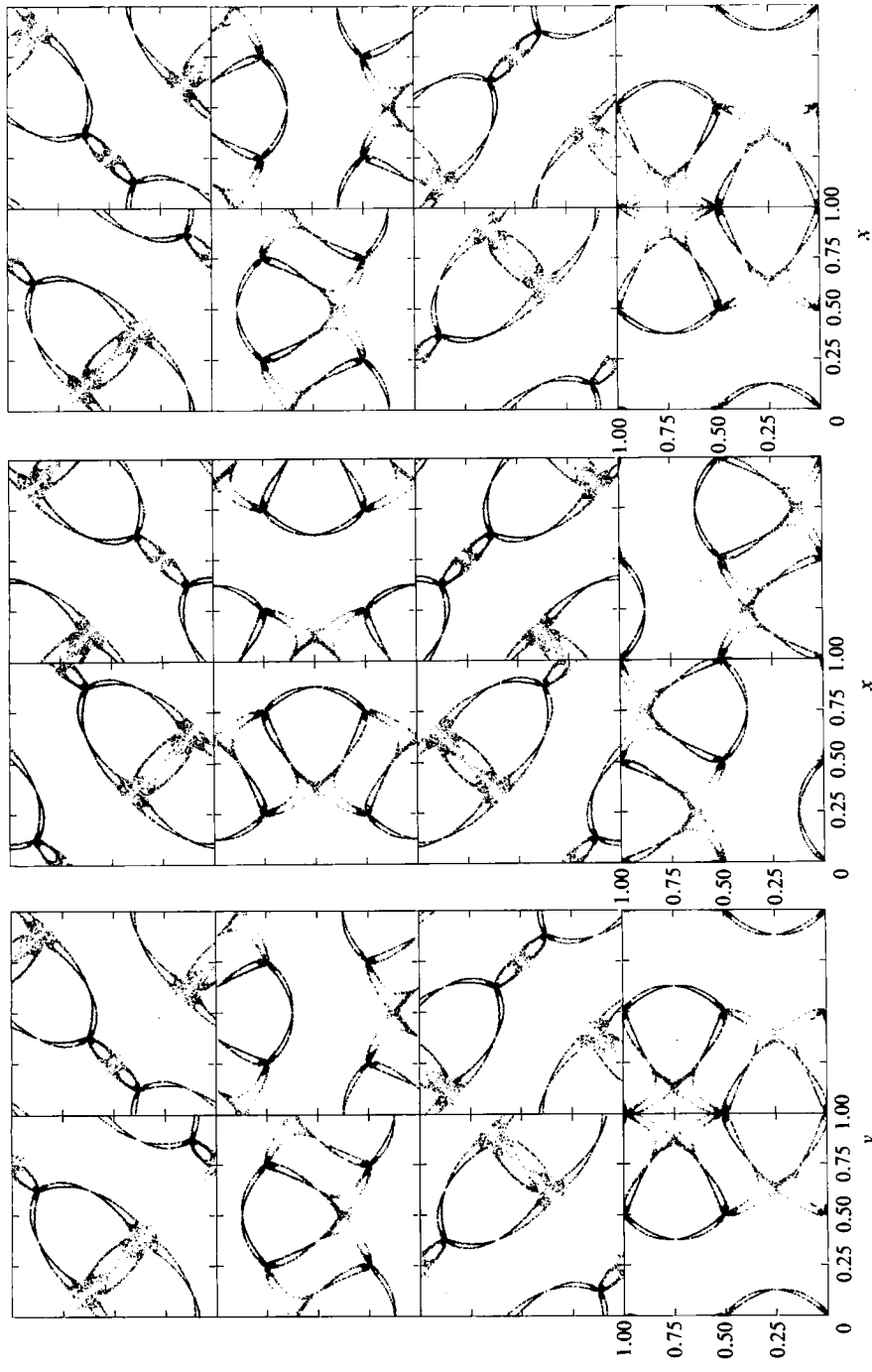

FIGURE 10. Poincaré section of a chaotic streamline for $A^2 = B^2 = C^2 = 1$.

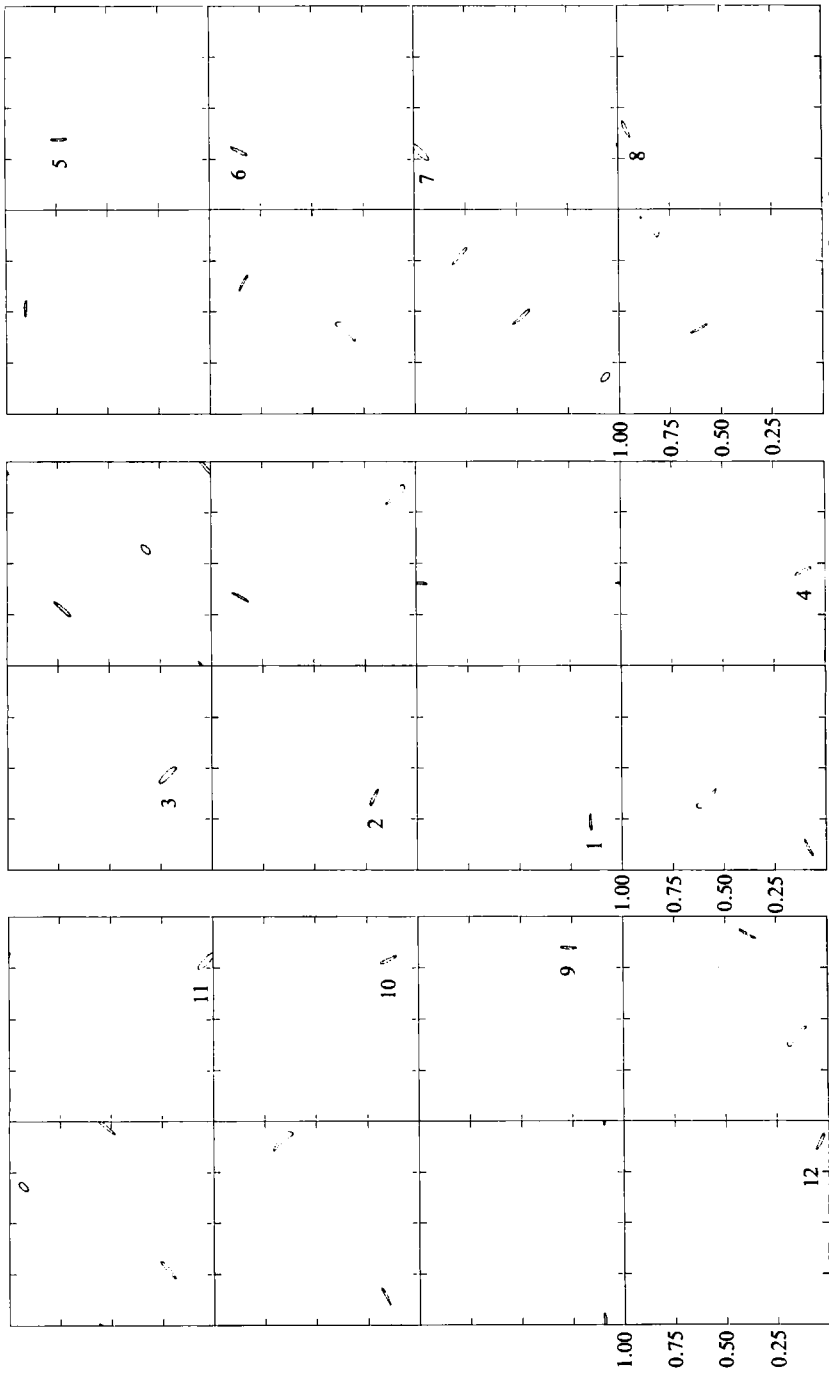

FIGURE 11. Poincaré section of a quasi-periodic streamline belonging to a secondary vortex, for $A^2 = B^2 = C^2 = 1$.

The particular case $A^2 = B^2 = C^2$ is invariant under cyclic permutation of the coordinates:

$$x' = z, \quad y' = x, \quad z' = y. \tag{3.2}$$

This explains why the sections of figure 10 look alike in the three directions. The vortex supporting the streamline of figure 11 is invariant under the transformation

$$x' = \pi - z, \quad y' = \pi + x, \quad z' = -y, \tag{3.3}$$

which is the product of the symmetries $S_1 S_3$ and (3.2). Another atypical feature of this symmetric case is that the one-dimensional unstable manifold of a type-α stagnation point coincides with the one-dimensional stable manifold of a type-β stagnation point (e.g. the line $x = y = z$). This configuration is clearly structurally unstable to perturbations of the coefficients A, B and C.

Figure 12 illustrates the case $A^2 = 1$, $B^2 = 1$, $C^2 = 0.5$, which lies inside the stagnation point region S of figure 2. The overall features are the same as in figure 7 but considerable fine structure appears in the chaotic region.

The case $A^2 = 1$, $B^2 = 0.5$, $C^2 = 0.5$ illustrated in figure 13 is quite similar to figure 7. Further cases with very small C will be shown in §4.

Taken together, our results suggest that the fundamental picture does not change significantly when the parameters are varied. The (x, y, z)-space is divided into (i) regions of regular, quasi-periodic streamlines; these regions consist essentially of the principal vortices; (ii) a chaotic region, which fills the space left free between the principal vortices and contains the stagnation points (when they exist). Of course, a finer analysis would almost certainly reveal additional structure on a smaller scale: small chaotic regions inside the vortices, small islands inside the large chaotic region, etc. as is usual in non-integrable systems.

Our numerical explorations have not revealed any new integrable cases other than the known cases ($C = 0$). This will be confirmed by further analytic studies in §§5 and 6.

3.2. *Resonances*

It is known from analytic work (see e.g. Arnold 1974, 1978) that KAM surfaces can be disrupted, leading to increased chaotic regions; this takes place through resonances (rational winding numbers). One of the most conspicuous cases is when a strong 3:1 resonance occurs at the centreline of the nested KAM surfaces forming one of the principal vortices. Figure 14 shows a Poincaré section in the $z = 0$ plane for $A = 1.19$, $B = 1.25$, $C = 0.18$, which is near a 3:1 resonance. We observe that the principal z-vortices have been disrupted and replaced by systems of three small vortices.

We made a systematic search for 3:1 resonances occurring at the centre of a principal vortex. Because of the symmetries (§2.2), it is sufficient to consider one particular vortex, provided that we abandon the constraints of the inequalities (2.15) but still normalize to $A = 1$. We select the y-vortex with y increasing. Again because of the symmetries, the centre of this vortex lies on the line $x = \frac{3}{2}\pi$ in the Poincaré section $y = 0$. For given parameters B and C, this centre is a fixed point of the Poincaré map defined by successive intersections with $y = 0$. Its z-coordinate is found by an iterative scheme. Next, the winding number at the fixed point is calculated by integrating two nearby orbits, starting with small opposite displacements ($\Delta z = 10^{-4}$) from the periodic orbit; this symmetrical scheme ensures an accuracy of order $(\Delta z)^2$ in the winding number. Then a search for a winding number of $\frac{1}{3}$ is made, again by an iteration scheme, holding C fixed and varying B. In the integrable case $C = 0$, the solutions for B are known (§4.3): they are $B = \frac{1}{2}(7 \pm 3\sqrt{5}) = 6.854102\ldots$ and $0.145898\ldots$. This provides starting points for the search.

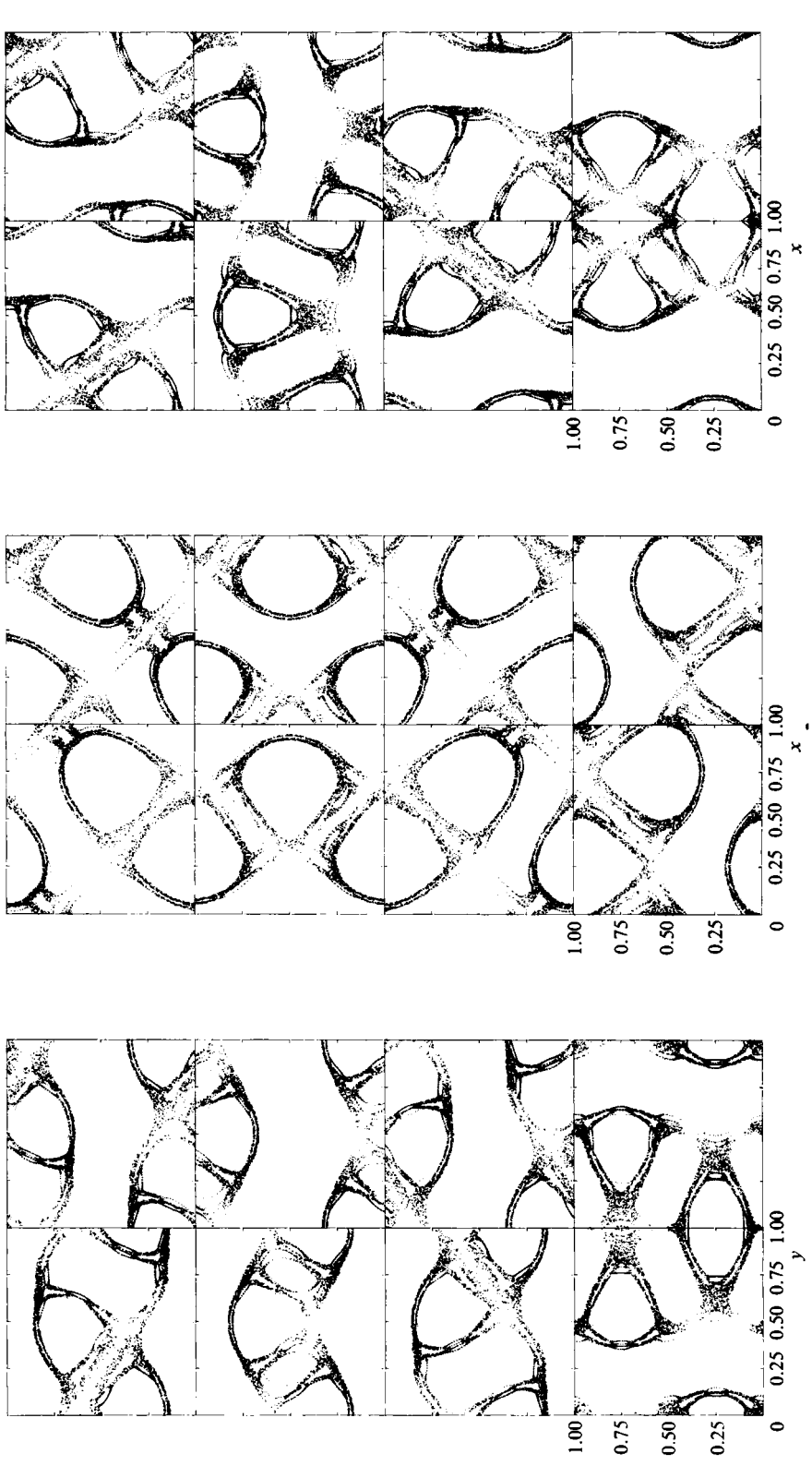

FIGURE 12. Poincaré section of a chaotic streamline for $A^2 = 1$, $B^2 = 1$, $C^2 = 0.5$.

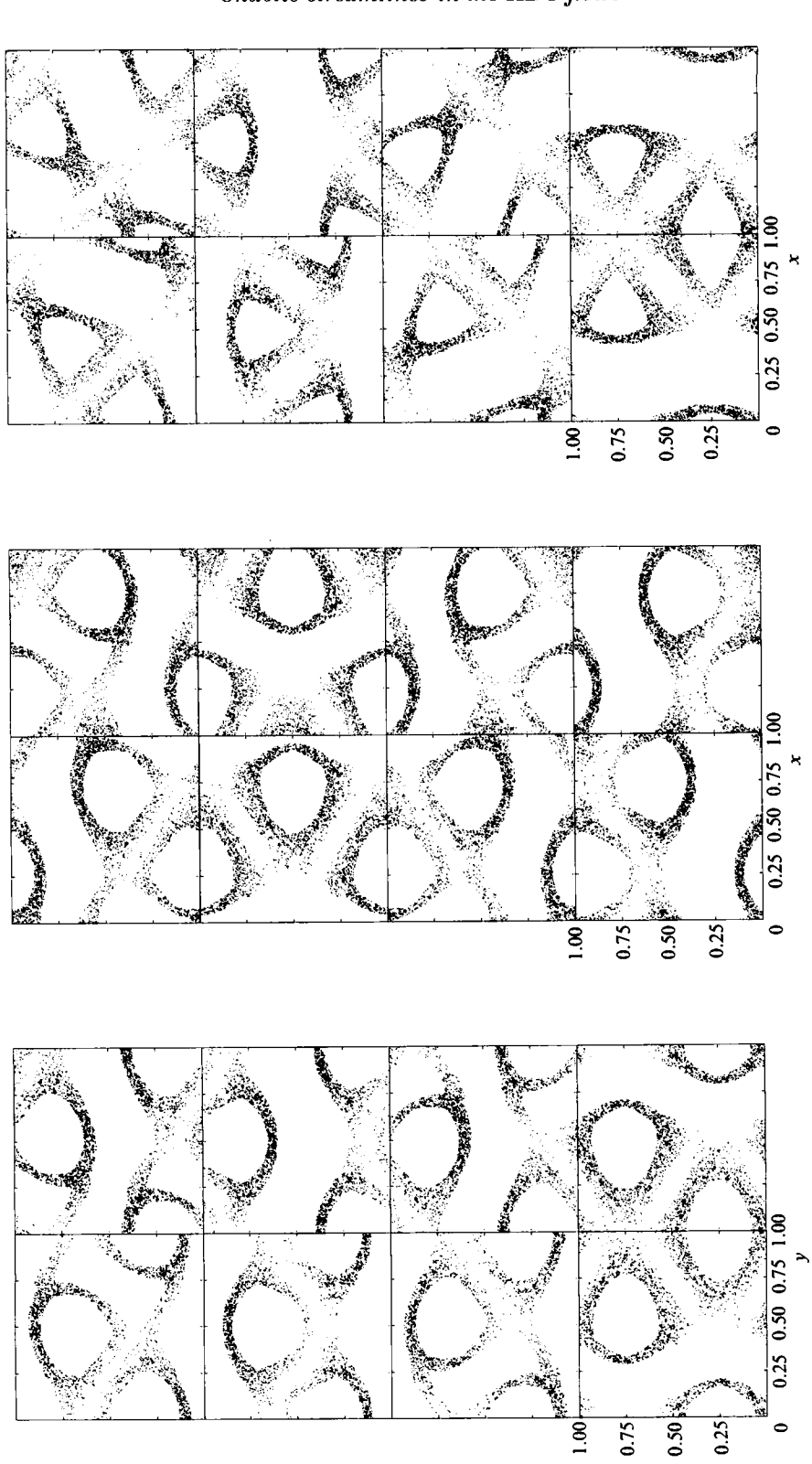

FIGURE 13. Poincaré section of a chaotic streamline for $A^2 = 1$, $B^2 = 0.5$, $C^2 = 0.5$.

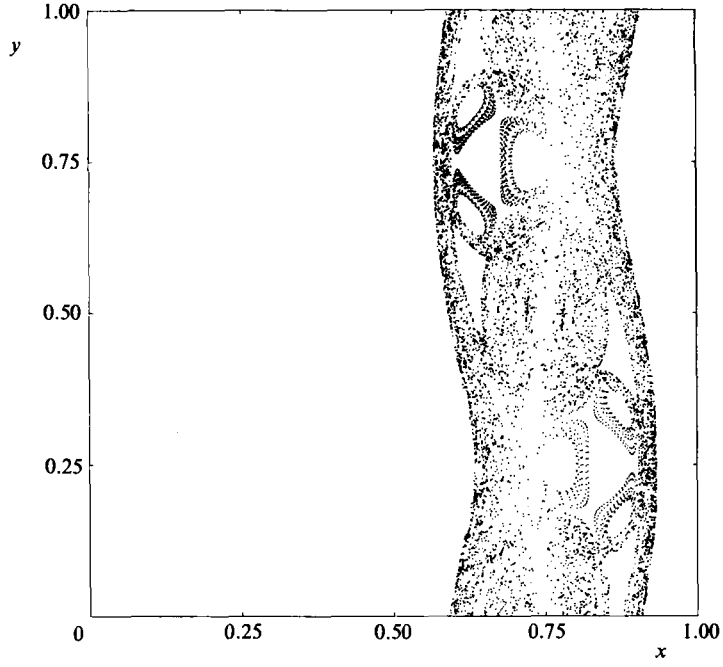

FIGURE 14. Poincaré section of a chaotic streamline in the vicinity of a 3:1 resonance.

Results are shown on figure 15 (solid line); points of interest are labelled P_1 to P_7. The locus of 3:1 resonances is a continuous curve joining the two starting points, P_1 and P_7. The left and right parts of this curve are exchanged under the symmetry (derived from (2.12), (2.13) and (2.14)):

$$A' = A = 1, \quad B' = \frac{1}{B}, \quad C' = \frac{C}{B}, \quad z' = \frac{3\pi}{2} - x, \quad x' = \frac{3\pi}{2} - z, \quad y' = \frac{3\pi}{2} - y. \tag{3.4}$$

This symmetry maps P_i into P_{8-i}; so it is only necessary to compute the left part of the curve, extending from P_1 to P_4. Note also that for any point of the curve, both y-vortices have a 3:1 resonance, since these vortices are exchanged under the S_2 symmetry (§2.2).

Finally we reintroduce the normalization (2.13), applying symmetries as needed. The curve of figure 15 is then folded into the solid line shown on figure 2. This line represents, in the reduced triangle, the locus of parameter values for which a 3:1 resonance exists for one pair of principal vortices. The direction of these vortices is indicated by X, Y, or Z. The X-segment is obtained from segment P_2P_3 of figure 15 by the symmetry (2.13); the Z-segment is obtained from segment P_3P_4 of figure 15 by the symmetry (derived from (2.12) and (2.14)):

$$A' = A = 1, \quad B' = \frac{1}{C}, \quad C' = \frac{B}{C}, \quad x' = z, \quad y' = x, \quad z' = y. \tag{3.5}$$

A noteworthy feature is that the resonance curve has a branch with B nearly constant (interval P_1P_3 in figure 15) close to the values of $\frac{1}{2}(7-3\sqrt{5})$ it achieves in the integrable case $C = 0$. An explanation of this feature follows from the perturbation theory result (4.15) of §4.3.

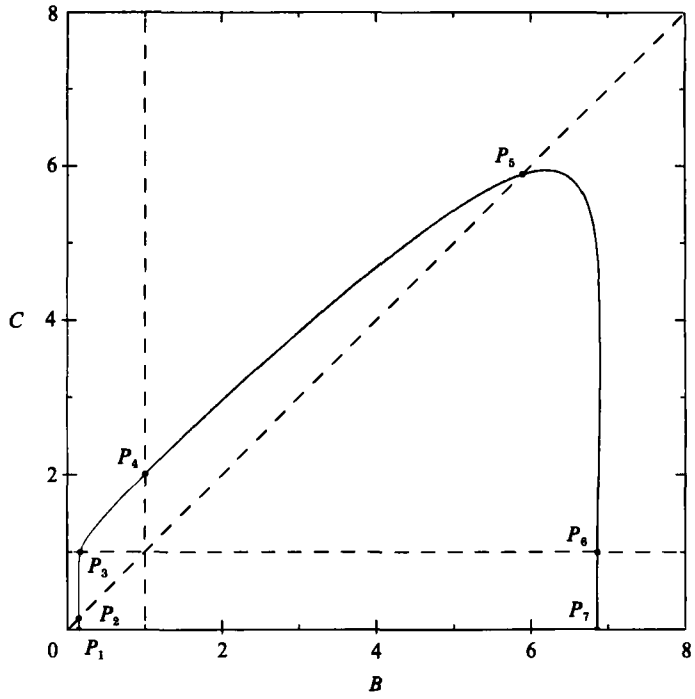

FIGURE 15. Locus of 3:1 resonances in parameter space.

Of particular interest are the 'double-resonance' points Q_2 and Q_3 of figure 2. Q_2 corresponds to $A = 1$, $B = C = 0.145789\ldots$; for these values of the parameters, the four principal vortices corresponding to the x- and y-directions all have a 3:1 resonance. Similarly at Q_3, which corresponds to $A = B = 1$, $C = 0.169834\ldots$, the four principal vortices in the x- and z-directions have a 3:1 resonance.

4:1 resonances can also produce chaos. Therefore their locus in the parameter plane was also calculated; it is shown as a dotted line in figure 2. The topology is the same as that of the 3:1 resonance. Inspection of the Poincaré sections shows, however, that the principal vortices are not destroyed in this case.

As for 2:1 resonances, numerical searches and analytical expansions indicate that they do not exist for real values of the parameters, except in the special integrable case $A = B = 1$, $C = 0$.

3.3 *Heteroclinic lines*

Heteroclinic lines (i.e. streamlines joining two stagnation points) and their possible relevance to the generation of chaos were discussed in §2.6. Here we show how their accurate numerical determination can be carried out and we give some results.

In this Section, we shall consider streamlines as existing in $\mathbf{R}^3$ rather than in $\mathbf{T}^3$. Generalizing (2.9), we call a *fundamental box* (k_x, k_y, k_z) the cube defined by

$$k_x\pi \leqslant x < (k_x+1)\pi, \quad k_y\pi \leqslant y < (k_y+1)\pi, \quad k_z\pi \leqslant z < (k_z+1)\pi, \tag{3.6}$$

with k_x, k_y, k_z integers. We shall also call *fundamental planes* the faces of the fundamental boxes.

It will be sufficient to search for the heteroclinic lines that have one end at a given stagnation point; all other heteroclinic lines can then be derived by use of the symmetries. We shall therefore consider only the heteroclinic lines starting from the stagnation point in the fundamental box (2.9), that is (0, 0, 0).

When stagnation points exist, there is one and exactly one in each fundamental box (excluding the borderline case which corresponds to the equality in (2.17)). Moreover, this point is of type β or α, depending on whether $k_x+k_y+k_z$ is even or odd. It follows that, when a streamline crosses a fundamental plane, it moves from a fundamental box occupied by an α-point to a box occupied by a β-point, or the converse.

A heteroclinic line must start from a β-point and end at an α-point. Therefore it crosses the fundamental planes an odd number of times. We designate this number by $2p-1$. The integer p will be called the *order* of the heteroclinic line; $p \geqslant 1$. We call P the point of the streamline corresponding to the central fundamental plane crossing, i.e. the pth crossing starting from either end. The streamline thus consists of two parts βP and $P\alpha$.

There exists a symmetry which brings α onto β (see §2.2). This symmetry transforms P into P', and $P\alpha$ into $\beta P'$, which is part of another streamline.

Consider the one-parameter set of all streamlines emerging from a given β-point along its two-dimensional unstable manifold. We choose a definite order p, and for each streamline we compute the point of intersection of rank p with the fundamental planes. These points form a set E_p, which consists of a number of disconnected curve segments. The following properties hold: to any heteroclinic line starting from β there corresponds a pair of points P, P' belonging to E_p, which are images of each other in a time-reversing symmetry. Conversely, a pair of points with these properties obviously produces a heteroclinic line.

The problem is thus reduced to finding pairs of image points in E_p. A simple way to do this is to 'normalize' the points P of E_p, i.e. to transform each point P into another point Q by the following series of steps: assume for instance that P lies in a fundamental plane $z = k\pi$;

(i) by an appropriate translation, bring the point in: $0 \leqslant x < 2\pi$, $0 \leqslant y < 2\pi$, $z = 0$ or π;

(ii) if $z = \pi$, bring the point on $z = 0$ by an application of S_2;

(iii) if $y < \frac{1}{2}\pi$ or $y > \frac{3}{2}\pi$, bring the point inside $\frac{1}{2}\pi \leqslant y \leqslant \frac{3}{2}\pi$ by S_1;

(iv) if $x < \frac{1}{2}\pi$ or $x > \frac{3}{2}\pi$, bring the point inside $\frac{1}{2}\pi \leqslant x \leqslant \frac{3}{2}\pi$ by S_3.

The end result of these manipulations is a point Q which lies in the square C_z defined by

$$\tfrac{1}{2}\pi \leqslant x \leqslant \tfrac{3}{2}\pi, \quad \tfrac{1}{2}\pi \leqslant y \leqslant \tfrac{3}{2}\pi, \quad z = 0. \tag{3.7}$$

Similar steps, deduced from the above by cyclic permutation of x, y, z, are taken if P lies in a plane $x = k\pi$ or $y = k\pi$, and produce a point Q lying in a square C_x or C_y.

The points Q thus obtained form a new set F_p, which again consists of a number of curve segments. It is easily shown that two points P, P' of E_p, which can be deduced from each other by a symmetry, have the same image Q in F_p. We have thus a computational strategy for finding all heteroclinic lines of order p: integrate numerically the streamlines starting from the β-point, and obtain the E_p set; apply the above steps to derive the F_p set; and look for curve intersections in that set. Each such intersection corresponds to one heteroclinic line.

In practice the family of streamlines emanating from the β-point is conveniently generated by taking as initial point for the numerical integration:

$$\beta + \epsilon_1 V_1 \cos\theta + \epsilon_2 V_2 \sin\theta, \tag{3.8}$$

where β represents the initial stagnation point, V_1 and V_2 are two eigenvectors corresponding to the two positive eigenvalues, ϵ_1 and ϵ_2 are small constants, and the parameter θ is varied from 0 to 2π.

Computations were made for the case

$$A^2 = 1, \quad B^2 = 0.9, \quad C^2 = 0.8. \tag{3.9}$$

All heteroclinic lines up to order 5 were determined. For $p = 1, 2, 3, 4, 5$, the number of heteroclinic lines emanating from the β-point was found to be: 3, 3, 6, 6, 20 respectively. This suggests that the number of heteroclinic lines increases indefinitely as the order is increased. This is also suggested by intuitive considerations: the stagnation points belong to the chaotic region, therefore a streamline emanating from a stagnation point will tend to fill densely that region; in particular it will approach any other stagnation point as closely as desired, an infinite number of times. In every such case, a slight adjustment of initial conditions should then be sufficient to obtain an exact heteroclinic line.

Heteroclinic lines can be symmetric with respect to their central point P (in which case P and P' coincide) or asymmetric. The first asymmetric lines appear only at order 3, but their number increases rapidly with p. Out of the above total of 38 lines, 12 are symmetric and 26 are asymmetric.

We studied also the set of α stagnation points in which these heteroclinic lines end. No obvious pattern was found. One noticeable result is that more than one heteroclinic line can end in the same α-point. For instance, three of the above 38 lines connect the β-point in the $(0,0,0)$ box to the α-point in the $(0,0,1)$ box. An open question is whether, for specified starting and ending points in $\mathbf{R}^3$, there exists always one, many or infinitely many heteroclinic lines.

4. The near-integrable case

4.1. *Formulation*

Perturbation analysis near an integrable case is one of the few analytic tools available for studying chaotic systems. For $C = 0$, the ABC flow is integrable (§2.4 and Appendix A). The Poincaré map from the $y = 0$ plane to the $y = 2\pi$ plane can be expanded in powers of C for small C. Such an expansion is particularly simple if we restrict attention to the neighbourhood of the principal y-vortex, e.g. near $x = \frac{1}{2}\pi$ and $z = 0$. As in (A 5), we set

$$\lambda^2 = AB, \quad m^2 = B/A, \quad C = \lambda\epsilon \quad (m^2 < 1). \tag{4.1}$$

It is convenient for the perturbation calculation to use the modified dependent variables

$$\zeta_r = m^{\frac{1}{2}}(x - \tfrac{1}{2}\pi), \quad \zeta_i = \frac{z}{m^{\frac{1}{2}}} \tag{4.2}$$

and introduce the complex variable

$$\zeta = \zeta_r + i\zeta_i. \tag{4.3}$$

Substituting into the flow equations (2.5) gives

$$\left.\begin{aligned} \lambda^{-1}\dot{\zeta}_r &= \frac{1}{m^{\frac{1}{2}}} \sin(m^{\frac{1}{2}}\zeta_i) + \epsilon m^{\frac{1}{2}} \cos y, \\ \lambda^{-1}\dot{\zeta}_i &= -m^{\frac{1}{2}} \sin\left(\frac{\zeta_r}{m^{\frac{1}{2}}}\right) + \frac{\epsilon}{m^{\frac{1}{2}}} \sin y, \\ \lambda^{-1}\dot{y} &= m \cos\left(\frac{\zeta_r}{m^{\frac{1}{2}}}\right) + m^{-1} \cos(m^{\frac{1}{2}}\zeta_i). \end{aligned}\right\} \tag{4.4}$$

For $\epsilon = 0$ there is the exact solution $\zeta = 0$. For $\epsilon > 0$ and small we are interested in the solution with $|\zeta| = O(\epsilon)$. We thus set

$$\zeta(y) = \epsilon\xi(y), \quad y = y(t), \tag{4.5}$$

substitute back into (4.4) and expand everything to leading order in ϵ^2. Elimination of t gives the single equation

$$[1-\tfrac{1}{2}\epsilon^2\omega_0|\xi|^2+O(\epsilon^4)]\frac{\mathrm{d}\xi}{\mathrm{d}y} = \tfrac{1}{2}\omega_0^{\frac{1}{2}}[(1+2\omega_0)^{\frac{1}{2}}\mathrm{e}^{\mathrm{i}y}-(1-2\omega_0)^{\frac{1}{2}}\mathrm{e}^{-\mathrm{i}y}]$$
$$-\mathrm{i}\omega_0\,\xi+\frac{\mathrm{i}}{16}\epsilon^2[\tfrac{1}{3}(E_0\,\xi^3+\xi^{*3})+|\xi|^2(\xi+E_0\,\xi^*)]+O(\epsilon^4), \tag{4.6}$$

where the star denotes complex-conjugate and, as in (A 5)–(A 6),

$$\omega_0^{-1} = m^{-1}+m, \quad E_0 = (1-4\omega_0^2)^{\frac{1}{2}}. \tag{4.7}$$

In the limit $\epsilon\downarrow 0$, (4.6) becomes linear and has the general solution

$$\xi_0(y) = -\tfrac{1}{2}\mathrm{i}(a_+\mathrm{e}^{\mathrm{i}y}+a_-\mathrm{e}^{-\mathrm{i}y})+\hat{\xi}_0\,\mathrm{e}^{-\mathrm{i}\omega_0 y}, \tag{4.8}$$

where

$$a_\pm = \frac{(\omega_0^{-1}\pm 2)^{\frac{1}{2}}}{\omega_0^{-1}\pm 1} \quad (0<\omega_0\leqslant\tfrac{1}{2}) \tag{4.9}$$

and $\hat{\xi}_0$ is an arbitrary complex number. When $\hat{\xi}_0 = 0$ we have a 2π-periodic solution, i.e. a closed streamline (on the torus). The $\mathrm{e}^{\mathrm{i}y}$ (or $\mathrm{e}^{-\mathrm{i}y}$) term corresponds to a helix winding in the positive (or negative) direction around the y-axis. The combination gives a helix with elliptic base, the overall winding of which is in the positive direction because $a_+ > a_- \geqslant 0$. The term proportional to $\hat{\xi}_0$ gives the deviation from the helical closed streamline of neighbouring streamlines. These are also helical, but with *negative* winding since ω_0 is positive. When y varies from 0 to 2π neighbouring streamlines have turned by 2π, so that ω_0 is the *winding number* (in the linear approximation). Finally, we note that the lowest-order perturbation solution (4.8) becomes identical with the somewhat heuristically derived solution (2.28) if we set $\hat{\xi}_0 = \mathrm{i}a(AB)^{\frac{1}{2}}C^{-1}\mathrm{e}^{\mathrm{i}\phi}$.

4.2. *The 2π-periodic solution*

When $\epsilon > 0$, it is in principle possible to find the 2π-periodic orbit to all orders in ϵ^2. This may be done in two ways. One is a variational method based on the observation that closed streamlines of Beltrami flow are extremals of the circulation integral $\oint \boldsymbol{u}\cdot\mathrm{d}\boldsymbol{x}$ along arbitrary closed contours (Cary & Littlejohn 1983). More directly, one can look for solutions of (4.6) of the form

$$\xi = \tilde{\xi}(\omega_0,\epsilon;y) = \sum_{-\infty}^{\infty}\tilde{\xi}_n(\omega_0,\epsilon)\,\mathrm{e}^{\mathrm{i}(2n+1)y}, \tag{4.10}$$

where the order-one contribution is given by (4.8) with $\hat{\xi}_0 = 0$. The higher-order corrections are tedious and, in general, not particularly enlightening. An exception seems to be the calculation of the order-ϵ^2 correction for the special case $A = B$ (which has additional symmetries). It has $\omega_0 = \frac{1}{2}$ and the 2π-periodic solution (4.8) is $\xi_0(y) = -(\frac{1}{3}\mathrm{i})\,\mathrm{e}^{\mathrm{i}y}$. Substitution into (4.6) gives

$$\frac{\mathrm{d}\tilde{\xi}}{\mathrm{d}y}+\tfrac{1}{2}\mathrm{i}\tilde{\xi} = \tfrac{1}{2}\mathrm{e}^{\mathrm{i}y}+\frac{\epsilon^2}{6^3}[\tfrac{5}{2}\mathrm{e}^{\mathrm{i}y}+\tfrac{1}{6}\mathrm{e}^{-3\mathrm{i}y}] \tag{4.11}$$

with periodic solution

$$\tilde{\xi} = -\tfrac{1}{3}\mathrm{i}\left(1+5\frac{\epsilon^2}{6^3}\right)\mathrm{e}^{\mathrm{i}y}+\frac{\mathrm{i}}{15}\frac{\epsilon^2}{6^3}\mathrm{e}^{-3\mathrm{i}y}. \tag{4.12}$$

A noteworthy feature is that the order-ϵ^2 corrections have very small coefficients. This suggests that some properties valid in the integrable case may still be approximately valid when $\epsilon = O(1)$ and, in particular, when $A = B = C$ (i.e. $\epsilon = 1$).

4.3. *Resonances in the near-integrable case*

The streamlines close to the 2π-periodic streamline discussed above have the form

$$\xi = \tilde{\xi}+\hat{\xi}, \tag{4.13}$$

where the small perturbation $\hat{\xi}$ satisfies a linear equation (derived from (4.6)). Hence, according to Floquet theory, $\hat{\xi}$ can be written in the form

$$\hat{\xi} = \mathrm{e}^{-\mathrm{i}\omega y}\sum_{-\infty}^{\infty}\hat{\xi}_n(\omega_0,\epsilon)\,\mathrm{e}^{2\mathrm{i}ny}, \tag{4.14}$$

where ω, which stands for $\omega(\epsilon)$, is the winding number in the limit of vanishing amplitude, $|\hat{\xi}|\to 0$. When ϵ is small, (4.8) indicates that the series is dominated by the $\hat{\xi}_0$ term and that $\omega(0) = \omega_0$. The order-ϵ^2 corrections are generally of no great interest except perhaps in the case of resonance. For the 3:1 resonance ($\omega = \frac{1}{3}$), we find that

$$\omega_0 = \frac{1}{3}\left[1-\frac{\epsilon^2}{8^3}+O(\epsilon^4)\right] \tag{4.15}$$

with

$$m^2 = \frac{B}{A} = \tfrac{1}{2}(7-3\sqrt{5})\left[1-\frac{3}{\sqrt{5}}\left(\frac{\epsilon}{16}\right)^2+O(\epsilon^4)\right]. \tag{4.16}$$

When $\epsilon = 0$, this result agrees with the numerically obtained value $B = 0.145898\ldots$ in the borderline case $C = 0$ (§3.2). For finite ϵ, the contribution from the order-ϵ^2 term is extremely small indeed, consistent with the fact that the interval P_1P_3 in figure 15 is almost straight. For instance at P_2 we have $B = 0.145789\ldots$ (§3.2), which differs from the value at $C = 0$ by only $-0.000109\ldots$. Note that this is in good agreement with the correction term in (4.16), which evaluates to $-0.000111\ldots$.

Similar remarks hold for the 4:1 resonance, for which we have to leading order

$$\omega_0 = \tfrac{1}{4}, \quad m^2 = 7-4\sqrt{3}. \tag{4.17}$$

When the amplitude of $|\hat{\xi}|$ is increased from zero, (4.14) may be used as a first approximation to the solution, in the neighbourhood of the 3:1 resonance, provided that we allow for the possibility of weak dependence on y of the coefficients $\hat{\xi}_n$. So, if we choose

$$\omega_0 = \tfrac{1}{3}+(-\tfrac{1}{3}+\tfrac{5}{8}\delta)\frac{\epsilon^2}{8^3}+O(\epsilon^4), \tag{4.18}$$

where the constant δ measures the departure of ω_0 from the resonant value given by (4.15), we find that

$$\hat{\xi}_0 = \frac{3\sqrt{5}}{16}\eta \tag{4.19}$$

evolves slowly according to

$$\frac{8^4}{5\epsilon^2}\frac{\mathrm{d}\eta}{\mathrm{d}y}+\mathrm{i}(\delta-|\eta|^2)\,\eta+2\eta^{*2} = 0. \tag{4.20}$$

Written in the polar form

$$\eta = r\,\mathrm{e}^{\mathrm{i}\phi} \tag{4.21}$$

(4.20) reduces to a Hamiltonian system with integral

$$\tfrac{1}{4}r^4 + \tfrac{2}{3}r^3 \sin 3\phi - \tfrac{1}{2}\delta r^2 = H, \text{ a constant.} \tag{4.22}$$

As δ is increased from $-\infty$ three new vortices form, when $\delta = -1$, centred at $r = 1$, $\phi = \frac{1}{2}\pi$, $\frac{7}{6}\pi$ and $\frac{11}{6}\pi$. Their size increases until they merge, when $\delta = 0$, at the centre of the original vortex, $r = 0$. For $\delta > 0$, the original vortex re-emerges at the centre but with reversed circulation in the η-plane. Our three new vortices with centres at $r = 1 + (1+\delta)^{\frac{1}{2}}$, $\phi = \frac{1}{2}\pi$, $\frac{7}{6}\pi$ and $\frac{11}{6}\pi$ bound the central vortex and are confined to an expanded resonant surface. They are linked by junction streamlines at $r = -1 + (1+\delta)^{\frac{1}{2}}$, $\phi = \frac{1}{6}\pi$, $\frac{5}{6}\pi$ and $\frac{3}{2}\pi$.

In view of the very large size of the coefficient of $\mathrm{d}\eta/\mathrm{d}y$ in (4.20), the intensity of the effect just described is unlikely to be strong until ϵ is large. Such is the case for the Poincaré section shown in figure 14 for which $m^2 = 0.144$, $\epsilon^2 \approx 6.2938$ implying $\delta \approx 0.3217$. Though three vortices are clearly seen, the large amount of chaos presumably means that we are outside a régime in which our weakly nonlinear development is applicable. Further evidence of the failure of our theory in this parameter range is clear from figure 2. According to (4.16), the C-coordinate of the branch Q_2Q_3 should be decreasing slightly with increasing B. In fact the C-coordinate decreases until $B \approx 0.55$ and then increases. We can, therefore, anticipate that higher-order terms affect the results significantly and are responsible for the breakup at the edge of the vortices.

4.4. *Outside the principal vortex*

So far we have focused on the local behaviour near the centre of the principal y-vortex.The global behaviour in the near-integrable case (C very small) is easily investigated by the numerical technique discussed in §3.1. Figure 16 shows the usual Poincaré sections for $A^2 = 1$, $B^2 = 0.5001$, $C^2 = 0.0002$. There is a fairly conspicuous chaotic zone surrounding the two principal y-vortices; this chaos comes from the bifurcation of separatrices originating from the homoclinic loop in the integrable case (figure 3). There are two small x-vortices; however no z-vortex going through from $z = 0$ to 2π is visible. In the integrable case, the solution for which is known in terms of elliptic functions, we can identify an imaginary centre streamline of a z-vortex (in the sense that it is linked with complex sn's). In that case the z-vortex is absent but the interpretation has interesting consequences which are discussed in Appendix A.

When C is increased starting from $C = 0$, the principal x-vortices arise from the streamlines marked (a) in figure 3, lying in the shear layers midway between the y-vortices. The corresponding winding numbers are zero so that these streamlines close after looping once in the x-direction. When perturbed with a small value of C, one of these lines with a particular value of y becomes the centre of a vortex, and another the junction of the separatrices that mark the vortex border.

More generally, for $C = 0$ there exist streamlines in the shear layer which close after p loopings in x and q loopings in y, where p and q are arbitrary integers. For very small C and fixed p and q, some of these lines go over as before into respectively centrelines of vortices and junctions of separatrices. However, numerical exploration indicates that, except for the principal one, these vortices are destroyed at quite small values of C. This happens as follows: the centreline is a periodic orbit which, as C increases, undergoes successive period-doubling bifurcations, leading to chaotic orbits

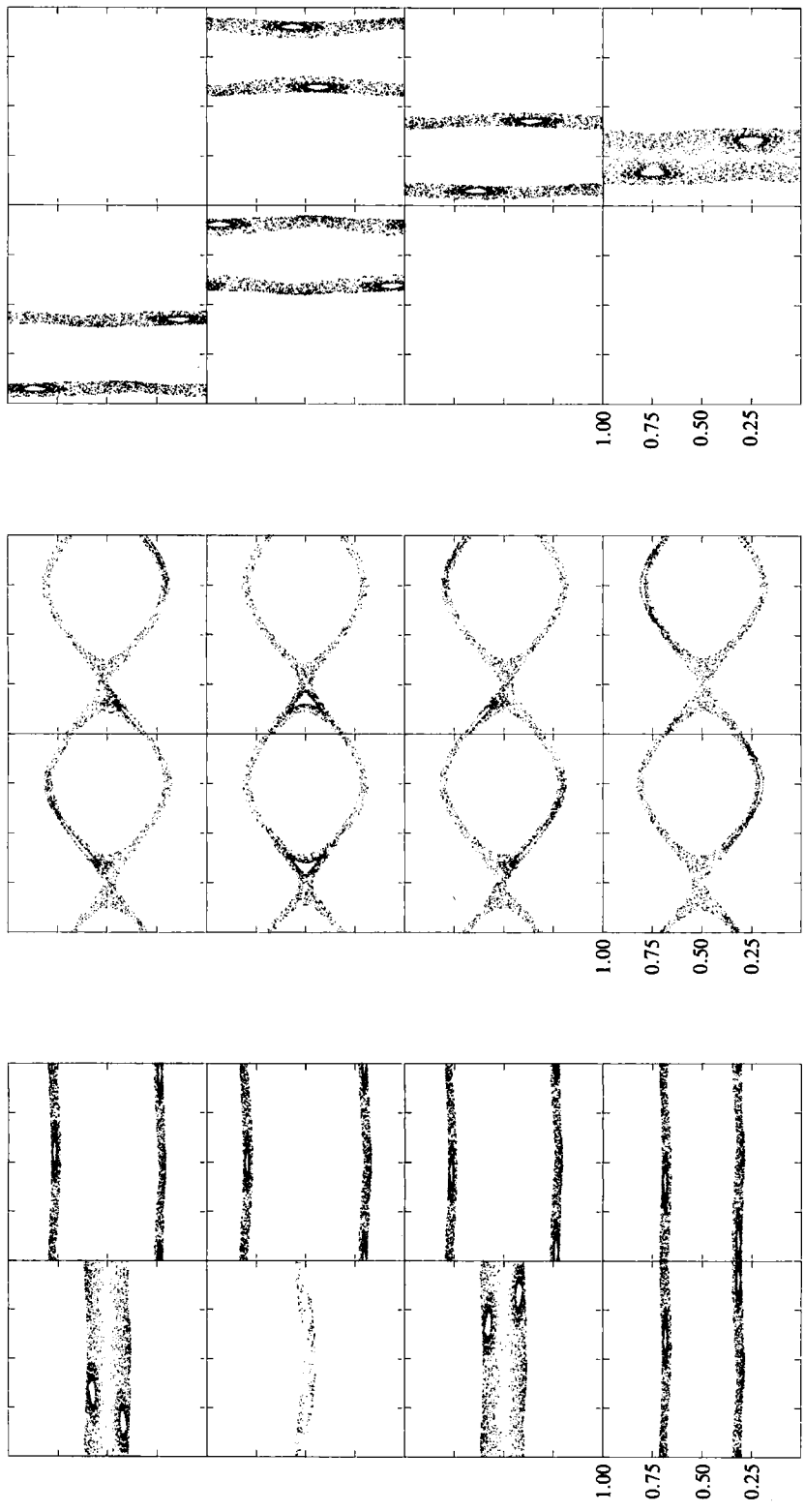

FIGURE 16. Poincaré section of a chaotic streamline in the near-integrable case $A^2 = 1$, $B^2 = 0.5001$, $C^2 = 0.0002$.

at a finite C (Collet, Eckmann & Koch 1983; Greene *et al.* 1983). Thereby the shear layer outside the principal vortices becomes chaotic.

The z-directed principal vortices are born in a tangent or saddle-node bifurcation (see Guckenheimer & Holmes 1983) at a modest value of C. For example, these vortices come into existence near $A^2 = 1$, $B^2 = \frac{2}{3}$, $C^2 = 0.013$, $x/2\pi = 0.7815$, $y/2\pi = 0.25$, and $x/2\pi = 0.7185$, $y/2\pi = 0.75$.

5. Search for integrable cases by Painlevé tests

Performing Painlevé tests seems at the moment the only non-numerical systematic method that can give hints of integrability. The method goes back to the work of Painlevé (1897) and Kowalevskaya (1889, 1890) who realized that a complete understanding of the analytic structure in the complex time-domain of a dynamical system governed by an o.d.e. can be as helpful as having integrability in the sense of that time (i.e. reduction to 'known' functions). Actually Painlevé proposed to extend the definition of integrability to include those o.d.e.'s for which the only movable singularities (i.e. depending on initial data) are poles. This is the case of the celebrated Painlevé transcendants, the simplest of which is the solution of

$$\ddot{x} = 6x^2 + t. \tag{5.1}$$

We briefly summarize the essential steps for this example, since this will simplify the subsequent explanations in connection with ABC flows (for details see Painlevé 1897 or Hille 1976). Dominant balance requires that near a singularity t_* we have $x(t) \simeq (t-t_*)^{-2}$. It is now assumed that $x(t)$ has an expansion near t_* of the form

$$x(t) = (t-t_*)^{-2} \sum_{j=0}^{\infty} u_j (t-t_*)^j. \tag{5.2}$$

Substitution into (5.1) gives the relation ($j = 1, 2, \ldots$)

$$(j^2-5j-6)\,u_j = 6 \sum_{\substack{0<r<j-1 \\ 0<s<j-1 \\ r+s=j}} u_r u_s + t_* \delta_{j,4} + \delta_{j,5}. \tag{5.3}$$

Since the right-hand side of (5.3) involves only the u_n ($n < j$), the relation can be solved recursively except when j^2-5j-6 vanishes for some integer. This happens at the 'resonance' $j = 6$ (sometimes also called Kowalevskaya exponent, cf. Yoshida 1984). The interesting observation (requiring a few lines of easy algebra) is that the right-hand side of (5.3) also vanishes at $j = 6$; the fulfilment of this compatibility condition implies that an arbitrary constant can be introduced for u_6; together with the arbitrary choice of t_* this gives two arbitrary constants, as required for the general solution of a second-order equation.

This subject has undergone a recent revival when it was realized that there may be a connection between the Painlevé property (and various generalizations thereof) and integrability in one of the modern senses for both o.d.e.'s and p.d.e's (Nakach 1977; Ablowitz, Ramani & Segur 1978, 1980; Ziglin 1981; Weiss, Tabor & Carnevale 1983; Jimbo, Kruskal & Miwa 1982; Ramani, Dorizzi & Grammaticos 1982; Lochak 1985 and references therein).

Particle trajectories for the ABC flows cannot have any singularities in the real domain but their analytic continuation to complex times may (and usually will) become singular. Complex-time singularities are of interest for other reasons than Painlevé tests. It has been shown by Frisch & Morf (1981) that high-frequency

intermittent bursts of the kind observed by Batchelor & Townsend (1949), Kuo & Corrsin (1971), Gagne (1980) and others can be related to complex-time singularities: when a real analytic signal (recorded, for example, by a probe in a turbulent fluid) is high-pass filtered with a cutoff Ω sufficiently large, the resulting signal displays bursts corresponding to the complex singularities closest to the real domain. Each burst has an amplitude proportional to $\exp(-\Omega|\tau_*|)$, τ_* being the imaginary part of the time of singularity. Particle trajectories in steady flows, which may be observed experimentally by tracking techniques, should also display such intermittent bursts.

In this and the following Section we investigate the nature of the complex-time singularities of the ABC flows. We begin by performing a Painlevé test. For this it is convenient to rewrite (2.5) in terms of new dependent variables defined as

$$\psi_n = \mathrm{e}^{\mathrm{i}x_n} \quad (n = 1,2,3). \tag{5.4}$$

We then obtain the system

$$\left.\begin{aligned} \psi_2\psi_3\dot{\psi}_1 &= [\tilde{A}\psi_2(\psi_3^2-1)+\mathrm{i}\tilde{C}(\psi_2^2+1)\psi_3]\psi_1, \\ \psi_3\psi_1\dot{\psi}_2 &= [\tilde{B}\psi_3(\psi_1^2-1)+\mathrm{i}\tilde{A}(\psi_3^2+1)\psi_1]\psi_2, \\ \psi_1\psi_2\dot{\psi}_3 &= [\tilde{C}\psi_1(\psi_2^2-1)+\mathrm{i}\tilde{B}(\psi_1^2+1)\psi_2]\psi_3, \end{aligned}\right\} \tag{5.5}$$

where $\tilde{A}$ (resp. $\tilde{B},\tilde{C}$) $=\frac{1}{2}A$ (resp. B,C). In the following we shall take $\tilde{A}\tilde{B}\tilde{C} \neq 0$ since we already know that the system is otherwise integrable. In the original system at a singularity at least one of the x_n variables must tend to infinity (otherwise it is easily shown, recursively, that all time derivatives are finite). In terms of the ψ_n this means that at least one of them must tend to infinity or zero. No loss of generality follows by assuming that the variable ψ_1 tends to infinity. Indeed the substitution

$$(\psi_1,\psi_2,\psi_3)\rightarrow(\psi_1^{-1},\psi_2^{-1},\psi_3) \tag{5.6}$$

is equivalent to

$$(x_1,x_2,x_3)\rightarrow(-x_1,-x_2,x_3) \tag{5.7}$$

which maps the (A,B,C) flow on the $(-A,B,-C)$ flow. There are similar transformations that leave ψ_1 or ψ_2 rather than ψ_3 invariant. Let us assume in the following that ψ_1 is the divergent variable (otherwise permute the variables). The leading-order behaviour near some singular time t_* is obtained by dominant balance analysis, making the substitution

$$\psi_1(t) = a(t-t_*)^\alpha, \quad \psi_2(t) = b(t-t_*)^\beta, \quad \psi_3(t) = c(t-t_*)^\gamma. \tag{5.8}$$

We first assume that all three terms are divergent, i.e. that

$$\mathrm{Re}\,\alpha, \mathrm{Re}\,\beta, \mathrm{Re}\,\gamma < 0. \tag{5.9}$$

This leads to the equation

$$(\alpha-1)(t-t_*)^{\alpha+\beta+\gamma-1} \simeq [\tilde{A}c(t-t_*)^{\alpha+\beta+2\gamma}+\mathrm{i}\tilde{C}b(t-t_*)^{\alpha+2\beta+\gamma}] \tag{5.10}$$

and two other equations deduced by cyclic permutation. The unique solution is

$$\alpha = \beta = \gamma = -1 \tag{5.11}$$

$$a = -\frac{1-\mathrm{i}}{2\tilde{B}}, \quad b = -\frac{1-\mathrm{i}}{2\tilde{C}}, \quad c = -\frac{1-\mathrm{i}}{2\tilde{A}}. \tag{5.12}$$

We then seek for ψ_1,ψ_2,ψ_3 and expansion near t_* of the form

$$\psi_1(t) = \sum_{j=0}^{\infty} a_j(t-t_*)^{j-1}, \quad \psi_2(t) = \sum_{j=0}^{\infty} b_j(t-t_*)^{j-1}, \quad \psi_3(t) = \sum_{j=0}^{\infty} c_j(t-t_*)^{j-1}. \tag{5.13}$$

We obtain by substitution into (5.5) the recursion relations for $j \geqslant 1$

$$\begin{pmatrix} 2j & 1+\mathrm{i} & 1-\mathrm{i} \\ 1-\mathrm{i} & 2j & 1+\mathrm{i} \\ 1+\mathrm{i} & 1-\mathrm{i} & 2j \end{pmatrix} \begin{pmatrix} a_j \\ b_j \\ c_j \end{pmatrix} = (R_j)\{a_k, b_k, c_k, k < j\}, \tag{5.14}$$

where for the sake of conciseness the expression of the vector R_j in the right-hand side has not been written. The resonances correspond to the vanishing of the determinant of the matrix in the left-hand side. This happens for

$$j = -1, \quad j = j_\pm = \frac{1 \pm \sqrt{3}}{2}. \tag{5.15}$$

The resonances $j = -1$ and j_- are not acceptable because they imply a stronger divergence than the leading order. The j_+ resonance allows the additional introduction in the expansion (5.13) of terms with the non-integer power j_+ (and multiples thereof); the only restriction on their coefficient set (a_{j+}, b_{j+}, c_{j+}) is that it belongs to the null-space of the corresponding matrix. This gives one arbitrary constant. Together with the arbitrary choice of t_* we have *two* arbitrary constants. However, we need *three* to describe the general solutions of (5.5). So, our starting point, the Ansatz (5.9) fails.

Next we relax the assumption that all three exponents α, β and γ have strictly negative real parts and look for solutions of the form

$$\psi_1(t) \sim a(t-t_*)^{-1}, \quad \psi_2(t) \sim b(t-t_*)^{-1}, \quad \psi_3(t) \sim c(t-t_*)^{\gamma} \tag{5.16}$$

with $\mathrm{Re}\,\gamma \geqslant 0$. With this Ansatz we find

$$a = -1/\tilde{B}, \quad b = \mathrm{i}/\tilde{C}, \quad \gamma = 0 \quad \text{and} \quad c \text{ arbitrary}. \tag{5.17}$$

We then look for expansions of the form

$$\psi_1(t) = \sum_{j=0}^{\infty} a_j (t-t_*)^{j-1}, \quad \psi_2(t) = \sum_{j=0}^{\infty} b_j (t-t_*)^{j-1}, \quad \psi_3(t) = \sum_{j=0}^{\infty} c_j (t-t_*)^{j}, \tag{5.18}$$

and obtain the new set of recursion relations for $j \geqslant 1$

$$\begin{pmatrix} jbc & ac & 0 \\ bc & jac & 0 \\ ibc & -iac & jab \end{pmatrix} \begin{pmatrix} a_j \\ b_j \\ c_j \end{pmatrix} = (S_j)\{a_k, b_k, c_k, k < j\}. \tag{5.19}$$

Now resonances occur for $j = -1$, 0 and $+1$. The value $j = 0$ reflects the arbitrary choice of c. We only need to consider $j = 1$ and to check whether compatibility conditions are fulfilled. By calculating explicitly the right-hand side of (5.19) we obtain

$$bca_1 + acb_1 = \tilde{A}(c^2-1)\,ab, \quad bca_1 + acb_1 = \mathrm{i}\tilde{A}(c^2+1)\,ab, \quad ibca_1 - iacb_1 + abc_1 = 0. \tag{5.20}$$

The first two equations are clearly incompatible for $\tilde{A} \neq 0$ and arbitrary c. As will be shown in §6, logarithmic corrections leading to breakdown of the Painlevé property are needed to ensure consistency and this introduces a third arbitrary constant. Hence we have found generic three-parameter expansions which do not satisfy the Painlevé property, and this for any values of A, B and C all different from zero. This suggests that the ABC flows present no further cases of integrability, other than the obvious ones.

Remarks. We have learned from V. I. Arnold (1985, private communication) of the existence of unpublished work of Ziglin, using a Painlevé-type analysis, which proves the non-integrability of the ABC flows for small C and the non-existence of integrals analytic in C.

H. Yoshida (1985, private communication) has noticed that ABC flows can be rewritten as a system of six first-order differential equations not involving A, B and C, with three first integrals depending on A, B and C. For this, in (2.5), set

$$p_1 = B\sin x, \quad p_2 = C\sin y, \quad p_3 = A\sin z, \tag{5.21}$$

$$q_1 = B\cos x, \quad q_2 = C\cos y, \quad q_3 = A\cos z, \tag{5.22}$$

to obtain

$$\left.\begin{aligned} \dot{p}_1 &= q_1(p_3+q_2), \quad \dot{p}_2 = q_2(p_1+q_3), \quad \dot{p}_3 = q_3(p_2+q_1), \\ \dot{q}_1 &= -p_1(p_3+q_2), \quad \dot{q}_2 = -p_2(p_1+q_3), \quad \dot{q}_3 = -p_3(p_2+q_1). \end{aligned}\right\} \tag{5.23}$$

In this form it is obvious that the Painlevé properties cannot depend on A, B and C as long as none of them vanishes.

6. Analytic structure and clustering of singularities

Several recent papers have been concerned with the structure of complex-time singularities in non-integrable cases (Tabor & Weiss 1981; Chang *et al.* 1981; Chang, Tabor & Weiss 1982; Chang *et al.* 1983; Yoshida 1984; Thual & Frisch 1984). In all cases studied so far it has been found that singularities are not isolated but form continuous singular sets which may constitute 'natural boundaries', i.e. boundaries across which analytic continuation is impossible.

We now show how it is possible to study the analytic structure of the ABC flows in the non-integrable cases using a technique developed by Tabor & Weiss (1981) for the Lorenz system. We begin by showing how logarithmic correction can cure the problem encountered at the non-compatible resonance $j = 1$ found in §5. Following, for example Bender & Orszag (1978, p. 164 example 5) we make the following assumption for the local behaviour of ψ_1, ψ_2, ψ_3 near t_*

$$\left.\begin{aligned} \psi_1(t) &= a(t-t_*)^{-1} + d\ln(t-t_*) + a_1 + \ldots, \\ \psi_2(t) &= b(t-t_*)^{-1} + e\ln(t-t_*) + b_1 + \ldots, \\ \psi_3(t) &= c + f(t-t_*)\ln(t-t_*) + c_1(t-t_*) + \ldots, \end{aligned}\right\} \tag{6.1}$$

where a and b are given by (5.17) and c is arbitrary. Balance of terms of order $(t-t_*)^{-2}$ in (5.5) requires now that

$$\left.\begin{aligned} bca_1 + acb_1 + bcd = \tilde{A}(c^2-1)ab, \quad bca_1 + acb_1 + ace = \mathrm{i}\tilde{A}(c^2+1)ab, \\ \mathrm{i}bca_1 - \mathrm{i}acb_1 + ab(c_1+f) = 0 \end{aligned}\right\} \tag{6.2}$$

and for the terms of order $(t-t_*)^{-2}\ln(t-t_*)$

$$ea + bd = 0, \quad abf = \mathrm{i}(ea-db)c. \tag{6.3}$$

From (6.2) and (6.3) we get

$$\left.\begin{aligned} d = a\tilde{A}[c(1-\mathrm{i}) - c^{-1}(1+\mathrm{i})], \quad e = -b\tilde{A}[c(1-\mathrm{i}) - c^{-1}(1+\mathrm{i})], \\ f = -\tilde{A}[c^2(1+\mathrm{i}) + (1-\mathrm{i})]. \end{aligned}\right\} \tag{6.4}$$

The conditions are now compatible and (a_1, b_1, c_1) is determined up to an arbitrary vector of the null-space of the matrix

$$\begin{pmatrix} bc & ac & 0 \\ bc & ac & 0 \\ ibc & -iac & ab \end{pmatrix}.$$

Together with t_* and c this yields the three expected arbitrary constants in the expansion about t_* which takes the general form (henceforth we set $t_* = 0$)

$$\psi_1 = \frac{1}{t}\sum_{k=0}^{+\infty}\sum_{j=0}^{+\infty} a_{kj} t^j (t\ln t)^k, \quad \psi_2 = \frac{1}{t}\sum_{k=0}^{+\infty}\sum_{j=0}^{+\infty} b_{kj} t^j (t\ln t)^k, \quad \psi_3 = \sum_{k=0}^{+\infty}\sum_{j=0}^{+\infty} c_{kj} t^j (t\ln t)^k. \tag{6.5}$$

We have verified by substitution of (6.5) into the basic equations (5.5) that the recursion relations giving the coefficient sets (a_{kj}, b_{kj}, c_{kj}) with $k+j = n$ in terms of $(a_{k'j'}, b_{k'j'}, c_{k'j'})$ with $k'+j' < n$ are well defined except when $k+j \leqslant 1$. But these particular values ($(k_{ij} = (0,0), (0,1), (1,0)$) correspond precisely to the orders of expansion just discussed.

At this point, following Tabor & Weiss (1981), we notice that terms containing powers of $t\ln t$ with no additional powers of t dominate for small t; hence we concentrate on those a_{kj}, b_{kj} and c_{kj} with $j = 0$. It is easily checked that a closed set of recursion relations is obtained for the a_{k0}, b_{k0} and c_{k0}. The solutions of these recursion relations are obtained by introducing the generating functions

$$\phi_1(x) = \sum_{k=0}^{\infty} a_{k0} x^k, \quad \phi_2(x) = \sum_{k=0}^{\infty} b_{k0} x^k, \quad \phi_3(x) = \sum_{k=0}^{\infty} c_{k0} x^k, \quad x = t\ln t. \tag{6.6}$$

Some algebra leads to the following set of differential equations:

$$x\frac{\mathrm{d}\phi_1}{\mathrm{d}x} - \phi_1 = \mathrm{i}\tilde{C}\phi_1\phi_2, \quad x\frac{\mathrm{d}\phi_2}{\mathrm{d}x} - \phi_2 = \tilde{B}\phi_1\phi_2, \quad x\frac{\mathrm{d}\phi_3}{\mathrm{d}x} = [\tilde{C}\phi_2 + \mathrm{i}\tilde{B}\phi_1]\phi_3. \tag{6.7}$$

The analogous system obtained by Tabor & Weiss (1981) had to be solved in terms of elliptic functions. Here the situation is simpler: the solution of (6.7) reads

$$\phi_1(x) = \lambda\tilde{B}^{-1}x\,\mathrm{e}^{-\lambda x}(\mathrm{e}^{-\lambda x}-1)^{-1}, \quad \phi_2(x) = -\mathrm{i}\lambda\tilde{C}x\,\mathrm{e}^{-\lambda x}(\mathrm{e}^{-\lambda x}-1)^{-1}, \quad \phi_3(x) = c\mathrm{e}^{-\mathrm{i}\lambda x}, \tag{6.8}$$

where

$$\lambda = \tilde{A}\left[\frac{1+\mathrm{i}}{c} - c(1+\mathrm{i})\right]. \tag{6.9}$$

It is seen that $\phi_1(x)$, $\phi_2(x)$ and $\phi_3(x)$ display to leading order the same sort of singularities in the x-plane as do ψ_1, ψ_2 and ψ_3 in the t-plane. The locations of the singularities (poles) nearest to $x = 0$ in the x-plane are

$$x_{*\pm} = \pm\frac{2\mathrm{i}\pi}{\lambda}. \tag{6.10}$$

Since $x = t\ln t$ is a multivalued function, each singularity in the x-plane gives rise in the t-plane to a sequence of secondary singularities converging to the original singularity at $t = 0$; their positions are the antecedents of $x_{*\pm}$ by the map $t \to t\ln t$. Since a similar analysis can be done starting from secondary singularities, and so on, a rather complicated recursive clustering of singularities is obtained. We believe that recursive clustering of singularities is a distinct mark of non-integrable systems. This may conceivably be (but has not yet been) related to the 'dense branching' of

integrals introduced by M. D. Kruskal (1984, Princeton University, unpublished work). He noticed that integrals of motion whose manifold of branches is so large that the possible values of the integrals become dense in the complex plane put essentially no restriction on the motion; hence his suggestion that non-integrability be defined by dense branching.

Finally we stress that expansions near complex singularities are of a purely local nature. It is somewhat surprising that local information (in the complex domain) can shed light on questions that are of a global nature (in the real domain) such as integrability.

This work was supported by the U.S. Department of Energy, Contract No. DE-AT03-84ER53158. We have benefitted from discussions with V. Arnold, S. Childress, D. Galloway, H. K. Moffatt, O. Thual, C. Tresser, and J. Weiss.

One of the authors of this paper, Albert Mehr, disappeared on 1 September 1984 in a mountain accident on Glacier d'Argentière. He was 25 years old. He had been studying at the Ecole Nationale Supérieure de Physique de Marseille. His Ph.D. work was done with D. Escande at the Ecole Polytechnique on transition to chaos in Hamiltonian systems with two degrees of freedom. He had many friends all over the world.

Appendix A. The integrable case

In this Appendix we discuss the exact solutions for the case $C = 0$. Then the equations for motion along the streamlines are

$$\dot{x} = A \sin z, \quad \dot{z} = B \cos x \quad (A \geqslant B > 0), \tag{A 1}$$

which have the invariant y-component of velocity

$$V = B \sin x + A \cos z. \tag{A 2}$$

Together with (A 1) it follows that

$$\phi_{\pm} = \tfrac{1}{2}(x - \tfrac{1}{2}\pi \pm z) \tag{A 3}$$

satisfies

$$\lambda^{-2}\dot{\phi}_{\pm}^2 = k^2 - \sin^2 \phi_{\pm}, \tag{A 4}$$

where

$$\left.\begin{aligned} &\lambda^2 = AB, \quad 4k^2 = \frac{1-E^2}{\omega_0^2}, \\ &E = \frac{V}{A+B}, \quad \omega_0^{-1} = m^{-1} + m, \quad m^2 = \frac{B}{A}. \end{aligned}\right\} \tag{A 5}$$

From (A 5) it is clear that the region inside the vortices with closed streamlines is distinguished by $|k| < 1$. The vortex centred at $x = \frac{1}{2}\pi$, $z = 0$ has the property $1 \geqslant E > E_0$, where

$$E_0 = \frac{A-B}{A+B}. \tag{A 6}$$

It is defined by the Jacobian elliptic function

$$\sin \phi_{\pm} = k \, \mathrm{sn}\,[\lambda(t \pm t_0)|k^2], \tag{A 7}$$

where, in view of (A 2), we have chosen our time origin so that $x = \frac{1}{2}\pi$, $z = z_0$ at $t = 0$ with z_0, t_0 the positive solutions of

$$k^{-2} \sin^2(\tfrac{1}{2}z_0) = \mathrm{sn}^2(\lambda t_0|k^2) = \frac{2m\omega_0}{1+E}. \tag{A 8}$$

It is straightforward to calculate the winding number of the streamflow within the vortex. The period of the flow in the y-direction is the periodicity length 2π divided by the velocity V. The period around the vortex obtained by integrating (A 4) is $4K(k^2)/\lambda$, where $K(k^2)$ is the complete elliptic integral of the first kind. The ratio of these two periods gives the winding number

$$\omega = \frac{\pi\omega_0 E^{-1}}{2K(k^2)}. \tag{A 9}$$

On the axis, $E = 1$, $k = 0$ we find that

$$\omega = \omega_0. \tag{A 10}$$

The shear layer outside the vortices is characterized by $|k| > 1$ with $E_0 > E > -E_0$. Applying Jacobi's real transformation (see, e.g., Abramowitz & Stegun 1964) (A 7) may be expressed in the alternative form

$$\sin\phi_{\pm} = \mathrm{sn}\,[\lambda k(t \pm t_0)|k^{-2}], \tag{A 11}$$

where (A 8) is now

$$\sin^2(\tfrac{1}{2}z_0) = \mathrm{sn}\,(\lambda k t_0|k^{-2}) = \frac{m(1-E)}{2\omega_0}. \tag{A 12}$$

When C is perturbed away from zero the streamline $E = 0$ becomes the centre of an x-directed principal vortex.

When $B = A$, the shear layer disappears ($E_0 = 0$) and when $B > A$ the shear layer becomes y-directed. Its description is readily obtained from (A 11) (A 12) by an appropriate change of variables. On the other hand, the solution (A 11)–(A 12) itself continues to be of interest. Note, however, that since $E_0 > E > -E_0$ it follows from (A 5) and (A 12) that

$$1 < \mathrm{sn}^2\,(\lambda k t_0|k^{-2}) < m^2. \tag{A 13}$$

Consequently the parameter t_0 is complex and so are the corresponding solutions (A 11). They are nevertheless of interest, because, for small finite values of C, two complex-conjugates can coalesce and form two real solutions. This 'tangent bifurcation' is the process by which the axes of the two z-directed principal vortices are formed.

Appendix B. Creation/destruction of stagnation points

Here we show a close connection between closed streamlines and streamlines that connect stagnation points of the flow (heteroclinic lines). In fact, we show that one kind of streamline can transform to the other when parameters are varied so that stagnation points are created or destroyed.

The technique that is used is perturbation theory. In particular, we study the parameter values $A^2 = 1, \frac{1}{2} < B^2 < 1$, and $C^2 = (1-B^2)(1+2\epsilon)$, where ϵ is small. When ϵ is negative, there are no stagnation points in the flow, but when it is small and positive they exist in close pairs. We proceed by examining the flow in a small region in the vicinity of the pair of stagnation points, and match these solutions to the global problem to obtain the desired streamlines.

When ϵ vanishes, there are four double stagnation points in the periodicity box. We focus on the one at $(\frac{1}{2}\pi, 0, \arccos(-B))$, with $\pi < z < \frac{3}{2}\pi$.

We first consider the local problem, and shift the origin of coordinates to the point where the stagnation points come into existence, $x = \frac{1}{2}\pi + X$, etc. Expanding, and

retaining leading-order terms with the Ansatz $X \approx Y \approx \epsilon^{\frac{1}{2}}$, $Z \approx \epsilon$, we find approximate equations for flow along the streamlines

$$\left.\begin{aligned} (1-B^2)^{-\frac{1}{2}}\frac{\mathrm{d}X}{\mathrm{d}t} &= \epsilon - TZ - \tfrac{1}{2}Y^2, \quad (1-B^2)^{-\frac{1}{2}}\frac{\mathrm{d}Y}{\mathrm{d}t} = Z - \tfrac{1}{2}TX^2, \\ (1-B^2)^{-\frac{1}{2}}\frac{\mathrm{d}Z}{\mathrm{d}t} &= Y - TX. \end{aligned}\right\} \tag{B 1}$$

Here $T \equiv B/(1-B^2)^{\frac{1}{2}}$. In the rest of this Appendix, an overdot represents the derivative with respect to the normalized time, $(1-B^2)^{\frac{1}{2}}t$. Within this approximation, the stagnation points occur at

$$X = \pm\frac{\epsilon^{\frac{1}{2}}}{T}, \quad Y = \pm\epsilon^{\frac{1}{2}}, \quad Z = \frac{\epsilon}{2T}. \tag{B 2}$$

The character of this flow can be better understood from the following two equations that can be derived from (B 1):

$$\dot{S}^{\pm} = C^{\pm}S^{\pm} \tag{B 3}$$

where

$$\left.\begin{aligned} S^{\pm} &= \pm(T^2+1)^{\frac{1}{2}}\left(Z-\frac{\epsilon}{2T}\right) + Y - TX \mp \frac{T}{6(T^2+1)^{\frac{5}{2}}}\Big[(T^4+2T^2+3) \\ &\quad -2T(T^2-1)\,XY(3T^4+2T^2+1)\,Y^2 + 3(T^2-1)(T^2+1)^2\frac{\epsilon}{T^2}\Big] + \ldots, \\ C^{\pm} &= \pm(T^2+1)^{\frac{1}{2}} + \frac{T}{3(T^2+1)^2}[T(T^2+2)\,X + (2T^2+1)\,Y] + \ldots. \end{aligned}\right\} \tag{B 4}$$

Here the dots stand for higher-order polynomials in X, Y and ϵ. They are determined by the condition in each order that the two error terms vanish, one independent of Z and the other linear in Z. It follows that streamlines can be confined to either of the surfaces $S^{\pm} = 0$. Streamlines away from the surface $S^{\pm} = 0$ diverge from it, while other streamlines converge toward $S^{-} = 0$. The two surfaces intersect orthogonally along a streamline. This line passes through the stagnation points when ϵ is positive.

Flow along the line of intersection can be deduced from the relation

$$\dot{X} + T\dot{Y} = \epsilon - \tfrac{1}{2}(T^2X^2 + Y^2). \tag{B 5}$$

Thus the flow is generally in the direction of negative X and Y, except between the two stagnation points when ϵ is positive. Note that characteristic rates for flow along the intersection streamline are small, of order ϵ and X, while the characteristic times for perpendicular flow are much faster, of order $C^{\pm}$.

We next consider the global problem when ϵ is negative, and search for closed streamlines that pass through the local region treated above. Now, the line $x = \frac{1}{2}\pi$, $y = 0$, or $X = Y = 0$, is a symmetry line of the system, according to §2, and it is shown in figure 1. Thus a streamline that connects this line with another symmetry line is necessarily a closed streamline, since symmetry forces the continuation of the flow to return to its starting point. We assume that there are closed streamlines that pass through the symmetry line for small Z. This is essentially equivalent to the statement that the surface $S^{-} = 0$, extended into the regime of finite X, Y, Z, intersects another symmetry line, since streamlines that pass through the symmetry line rapidly converge to $S^{-} = 0$. In the same way, by symmetry, the closed streamlines must come back into the local region very close to the surface $S^{+} = 0$. In the limit of small ϵ,

the ratio of velocities parallel and perpendicular to the intersection streamline becomes very large. Thus a streamline that heads out in a given direction to intersect a given symmetry line must come asymptotically close to the intersection streamline, and in the limit of vanishing ϵ, become coincident with it.

It is reasonably clear that the flow in the neighbourhood of this streamline must be globally unstable, since it is extremely unstable locally. Further, the period of the flow becomes infinite in the limit as ϵ goes to zero.

Finally, we consider the flow when ϵ is positive. The closed streamlines that were discussed in the previous paragraph do not exist here. To see this, note that the stagnation point at positive X and Y is a node of the flow in the $S^+ = 0$ surface. Thus it is a type-α point in the notation of §2.3. The flow diverges from this point along a line lying in the $S^- = 0$ surface, so that flow from upstream near the intersection of $S^\pm$ is blocked from the course it took in the negative-ϵ case.

Closed loops of streamlines can be formed in the following way. In the surface $S^- = 0$, flow diverges from the type-β stagnation point at negative X and Y. Any of these streamlines that intersect a symmetry line return to the type-α point discussed above, closely following the closed streamline that exists for negative ϵ. This can be closed by the streamline along the intersection of $S^\pm = 0$, that joins the two stagnation points.

Thus it is reasonable to say that closed streamlines can be replaced by heteroclinic lines when stagnation points are formed.

REFERENCES

Ablowitz, M. J., Ramani, A. & Segur, H. 1978 *Lett. Nuovo Cim.* **23**, 333.

Ablowitz, M. J., Ramani, A. & Segur, H. 1980 *J. Math. Phys.* **21**, 715 and **21**, 1006.

Abramowitz, M. & Stegun, I. A. 1964 *Handbook of Mathematical Functions.* Applied Math. Series **55**, National Bureau of Standards.

Aref, H. 1984 *J. Fluid Mech.* **143**, 1.

Arnold, V. I. 1965 *C.R. Acad. Sci. Paris* **261**, 17.

Arnold, V. I. 1974 *Les Méthodes Mathématiques de la Mécanique Classique.* Moscow: Mir. English translation *Mathematical Methods of Classical Mechanics.* Springer (1980).

Arnold, V. I. 1978 *Chapitres Supplémentaires de la Théorie des Equations Différentielles Ordinaires.* (Translated from Russian original.) Moscow: Mir.

Arnold, V. I. 1984 In *Nekotore Voprocy Sovremennovo Analisa*, p. 8. University of Moscow.

Arnold, V. I. & Korkina, E. I. 1983 *Vest. Mosk. Un. Ta. Ser. 1. Matematika Mecanika* **3**, 43.

Arnold, V. I., Zel'dovich, Ya.B., Ruzmaikin, A. A. & Sokolov, D. D. 1981 *Zh. Eksp. Teor. Fiz.* **81**, 2052; *Sov. Phys. JETP* **54**, 1083.

Arter, W. 1983 *Phys. Lett.* **97A**, 171.

Batchelor, G. K. & Townsend, A. A. 1949 *Proc. Roy. Soc. Lond.* **A199**, 238.

Bender, C. M. & Orszag, S. A. 1978 *Advanced Mathematical Methods for Scientists and Engineers.* McGraw Hill.

Birkhoff, G. D. 1927 *Dynamical systems.* American Mathematical Society.

Cary, J. R. & Littlejohn, R. G. 1983 *Ann. Phys.* **151**, 1.

Chang, Y. F., Greene, J. M., Tabor, M. & Weiss, J. 1983 *Physica* **8D**, 183.

Chang, Y. F., Tabor, M., Weiss, J. & Corliss, G. 1981 *Phys. Lett.* **A85**, 211.

Chang, Y. F., Tabor, M. & Weiss, J. 1982 *J. Math. Phys.* **23**, 531.

Childress, S. 1967 *Rep.* AFOSR-67-0124. Courant Institute, New York.

Childress, S. 1970 *J. Math. Phys.* **11**, 3063.

Collet, P., Eckmann, J.-P. & Koch, H. 1983 *Physica* **3D**, 457.

Cowley, S. W. H. 1973 *Radio Sci.* **8**, 903.

FRISCH, U. & MORF, R. 1981 *Phys. Rev.* **A23**, 2673.

GAGNE, Y. 1980 Intermittence en turbulence developpeé. Thesis, Institut de Mécanique de Grenoble, unpublished.

GALLOWAY, D. J. & FRISCH, U. 1984 *Geophys. Astrophys. Fluid Dyn.* **29**, 13.

GALLOWAY, D. J. & FRISCH, U. 1985 *The Hydrodynamic Stability of the ABC Flows.* Preprint.

GALLOWAY, D. J. & FRISCH, U. 1986 Dynamo action in a family of flows with chaotic streamlines. *Geophys. Astrophys. Fluid Dyn.* (To appear).

GAUTERO, J.-L. 1985 *C. R. Acad. Sci. Paris* **301**, 1095.

GREENE, J. M. 1982 In *Nonlinear Problems: Present and Future* (ed. A. Bishop, D. Campbell & B. Nicolaenko), p. 423. North-Holland.

GREENE, J. M., MACKAY, R. S., VIVALDI, F. & FEIGENBAUM, M. J. 1983 *Physica* **3D**, 468.

GUCKENHEIMER, J. & HOLMES, P. 1983 *Nonlinear Oscillations, Dynamical Systems, and Bifurcations of Vector Fields.* Springer.

HELLEMAN, R. H. G. 1980 In *Fundamental Problems in Statistical Mechanics* (ed. E. G. D. Cohen), vol. 5, p. 165. North-Holland.

HÉNON, M. 1966 *C.R. Acad. Sci. Paris* **262**, 312.

HÉNON, M. 1983 In *Chaotic Behaviour of Deterministic Systems, Les Houches Summer School, Session XXXVI* (ed. G. Iooss, R. H. G. Helleman & R. Stora), p. 55. North-Holland.

HILLE, E. 1976 *Ordinary Differential Equations in the Complex Domain.* Wiley.

IOOSS, G., HELLEMAN, R. H. G. & STORA, R. (ED.) 1983 *Chaotic Behaviour of Deterministic Systems, Les Houches Summer School, Session XXXVI.* North-Holland.

JIMBO, M., KRUSKAL, M. D. & MIWA, T. 1982 *Phys. Lett.* **A92**, 59.

KOWALEVSKAYA, S. 1889 *Acta Math.* **12**, 177.

KOWALEVSKAYA, S. 1890 *Acta Math.* **14**, 81.

KUO, A. Y. & CORRSIN, S. 1971 *J. Fluid Mech.* **50**, 285.

LANDAU, E. 1927 *Elementare Zahlentheorie.* Leipzig: Hirzel. Translated as *Elementary Number Theory*, (1958). Chelsea.

LOCHAK, P. 1985 *Phys. Lett.* **A108**, 188.

MELNIKOV, V. K. 1963 *Trans. Moscow Math. Soc.* **12**, 1.

MOFFATT, H. K. 1985 *J. Fluid Mech.* **159**, 359.

MOFFATT, H. K. & PROCTOR, M. R. E. 1985 *J. Fluid Mech.*, **154**, 493.

MOSER, J. 1973 *Stable and Random Motions in Dynamical Systems.* Princeton University Press.

NAKACH, R. 1977 In *Plasma Physics Nonlinear Theory and Experiments* (ed. H. Wilhelmson), p. 456, Plenum.

PAINLEVÉ, P. 1897 *Leçons sur la Théorie des Equations Différentielles.* Hermann.

PARKER, E. N. 1985 *Dynamical Nonequilibrium of Magnetic Fields With Arbitrary Interweaving of the Lines of Force.* Preprint, University of Chicago.

POINCARÉ, H. 1892 *Les Méthodes Nouvelles de la Mécanique Céleste.* Gauthier-Villars, Paris.

RAMANI, A., DORIZZI, B. & GRAMMATICOS, B. 1892 *Phys. Rev. Lett.* **49**, 1539.

ŠIL'NIKOV, L. P. 1969 *Dokl. Akad. Nauk SSSR* **189**; translation *Soviet Math.* **10**, 1368.

TABOR, M. & WEISS, J. 1981 *Phys. Rev.* **A24**, 2157.

THUAL, O. & FRISCH, U. 1984 *Natural Boundary in the Kuramoto Model.* In *Combustion and Nonlinear Phenomena, (Les Houches lectures)* (ed. P. Clavin, B. Larrouturou and P. Pelcé), Editions de Physique (Paris).

WEISS, J., TABOR, M. & CARNEVALE, G. 1983 *J. Math. Phys.* **24**, 522.

YOSHIDA, H. 1984 In *Chaos and Statistical Mechanics, Proc. Sixth Kyoto Summer Institute* (ed. Y. Kuramoto), p. 42. Springer.

ZEL'DOVICH, YA. B., RUZMAIKIN, A. A. & SOKOLOV, D. D. 1983 Magnetic Fields in Astrophysics. In *The Fluid Mechanics of Astrophysics and Geophysics*; vol. 3 (ed. P. H. Roberts). Gordon and Breach.

ZIGLIN, S. L. 1981 *Dokl. Akad. Nauk SSSR* **257**, no. 2; translation *Soviet Math.* **23**, 220.